Supplement materials for paper "Challenges of high-fidelity air quality modeling in urban environments - PALM sensitivity study during stable conditions"

Content

A. Synoptic situation

Figure S01: Surface pressure map and cloud cover over the Atlantic and Europe for 13 February 2023, 00 UTC. Data source CHMI.
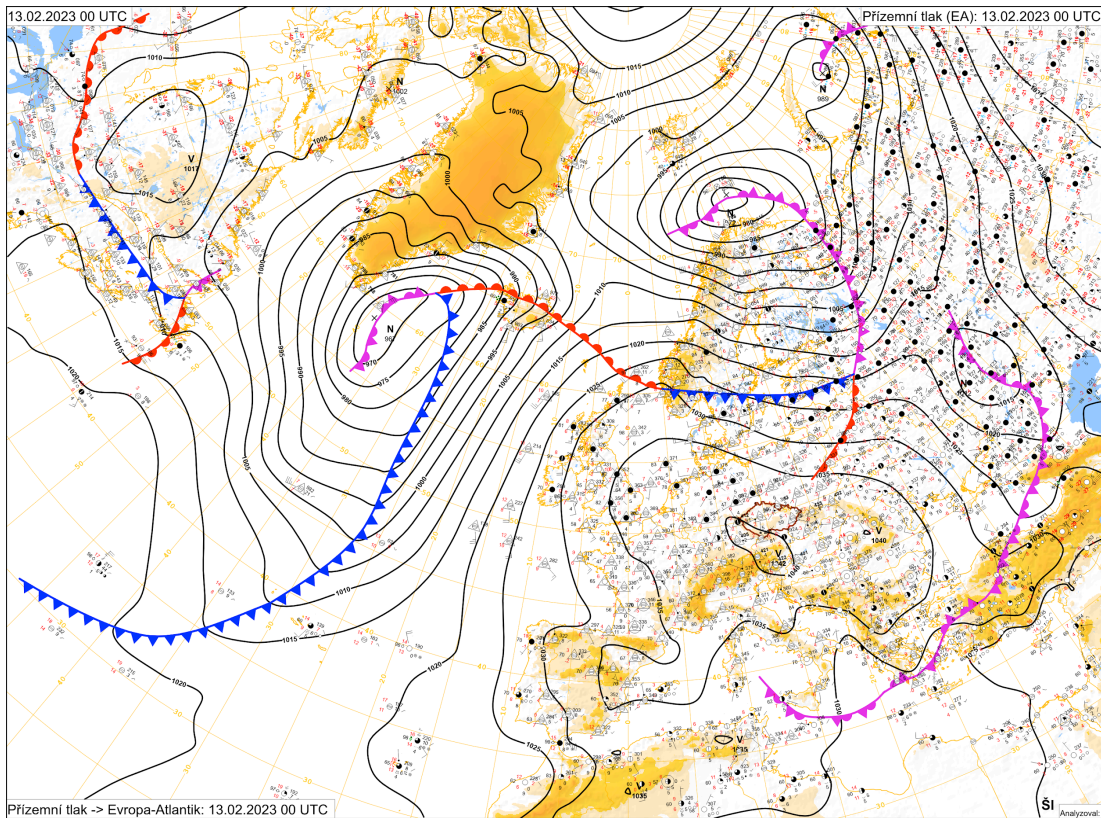

Figure S02: Surface pressure map and cloud cover over the Atlantic and Europe for 13 February 2023, 06 UTC. Data source CHMI.
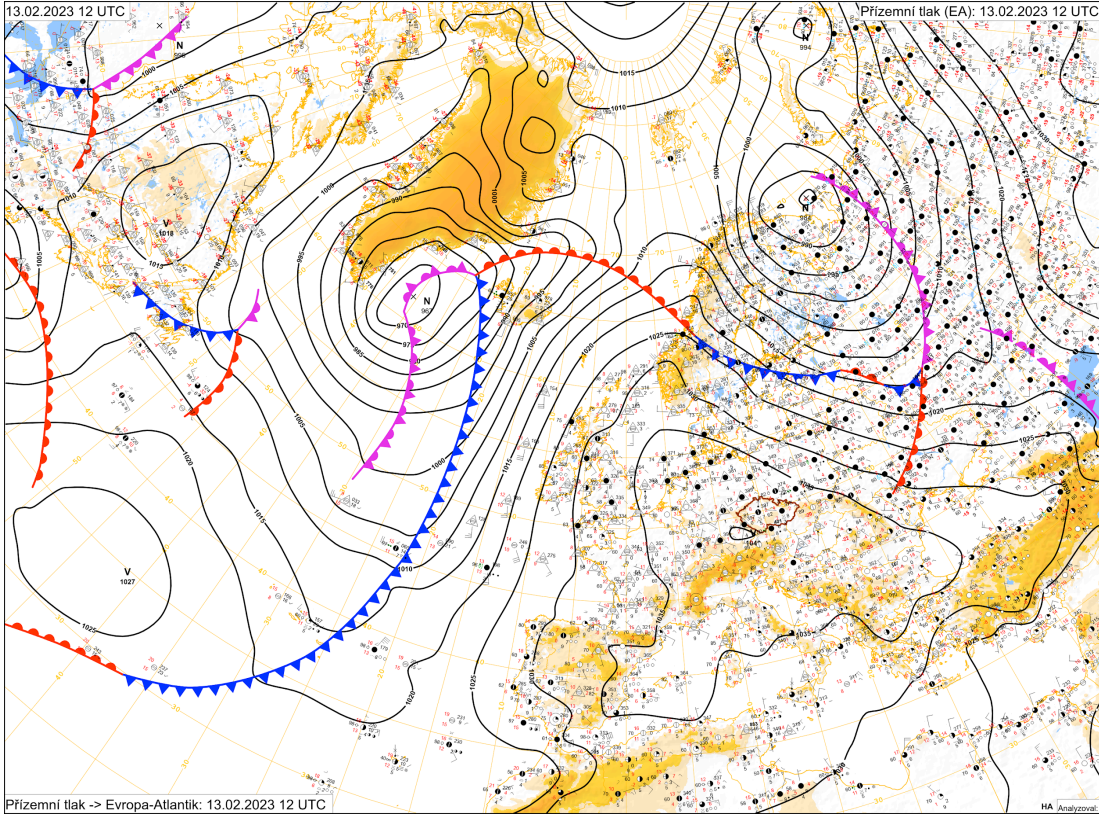
Figure S03: Surface pressure map and cloud cover over the Atlantic and Europe for 13 February 2023, 12 UTC. *Data source CHMI.*
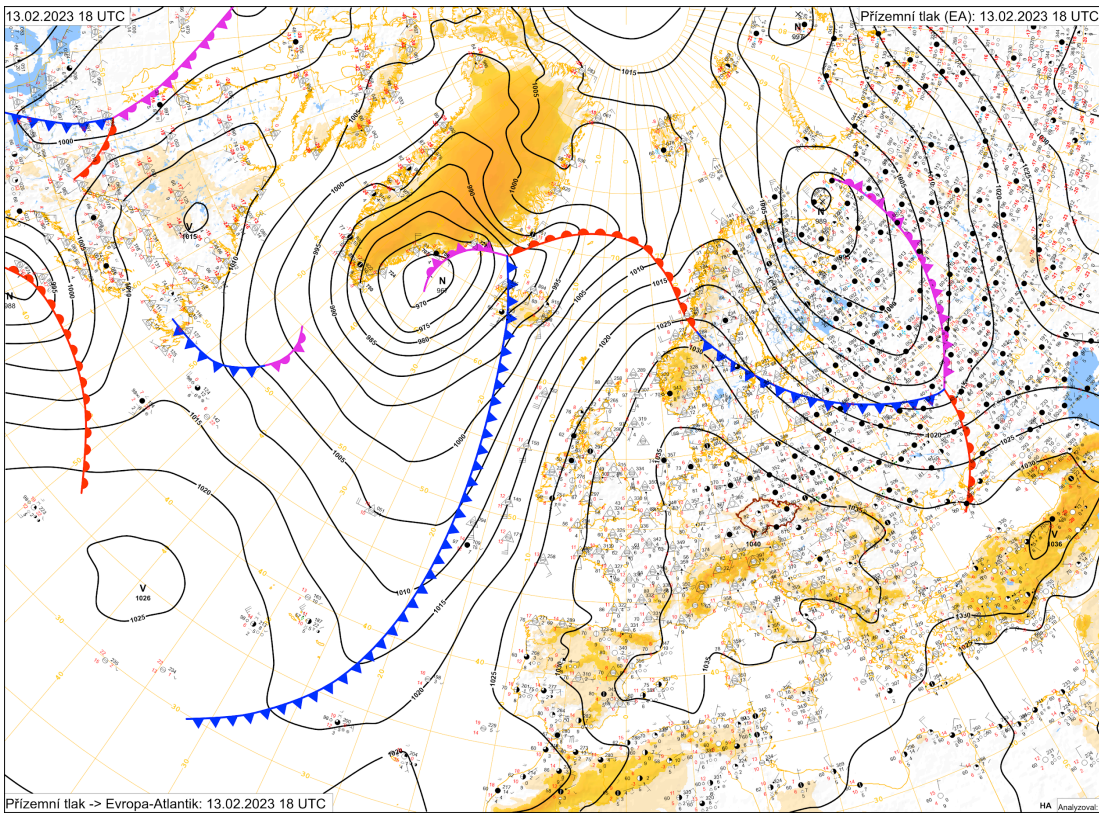
Figure S04: Surface pressure map and cloud cover over the Atlantic and Europe for 13 February 2023, 18 UTC. Data source CHMI.
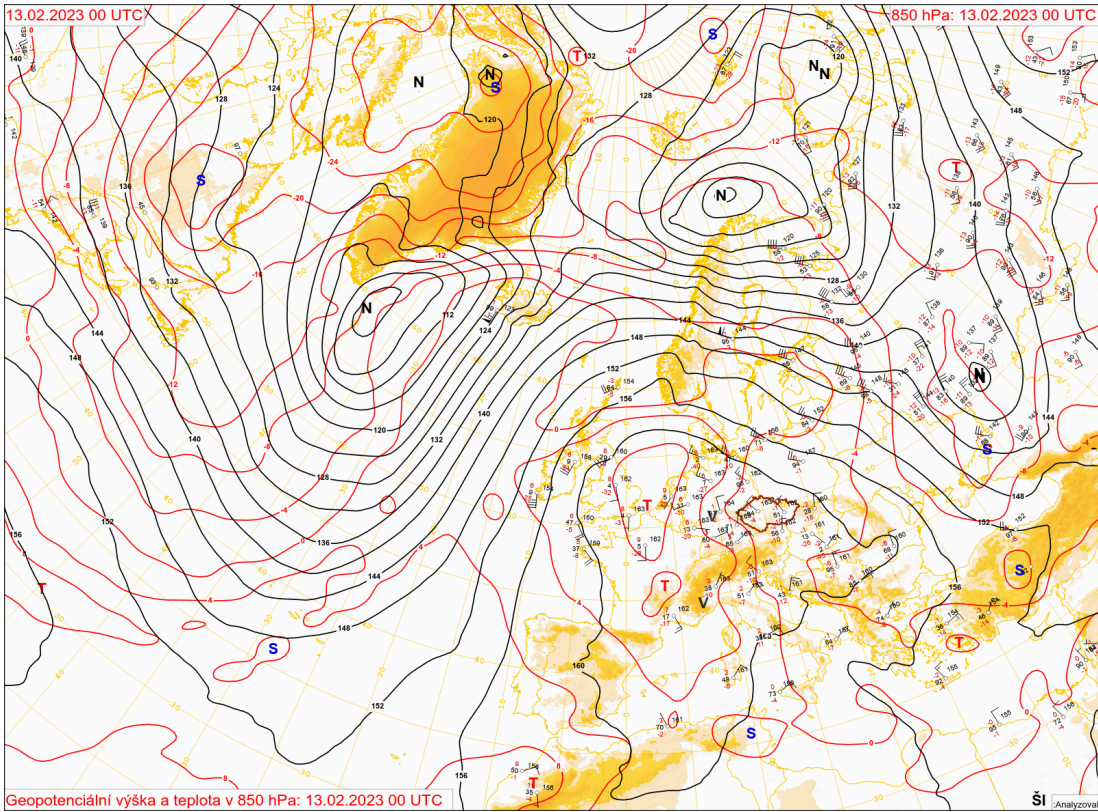
Figure S05: Geopotential height (black) and temperature (red) at 850 hPa for 13 February 2023, 00 UTC. N: cyclone, V: anticyclone. Data source CHMI.
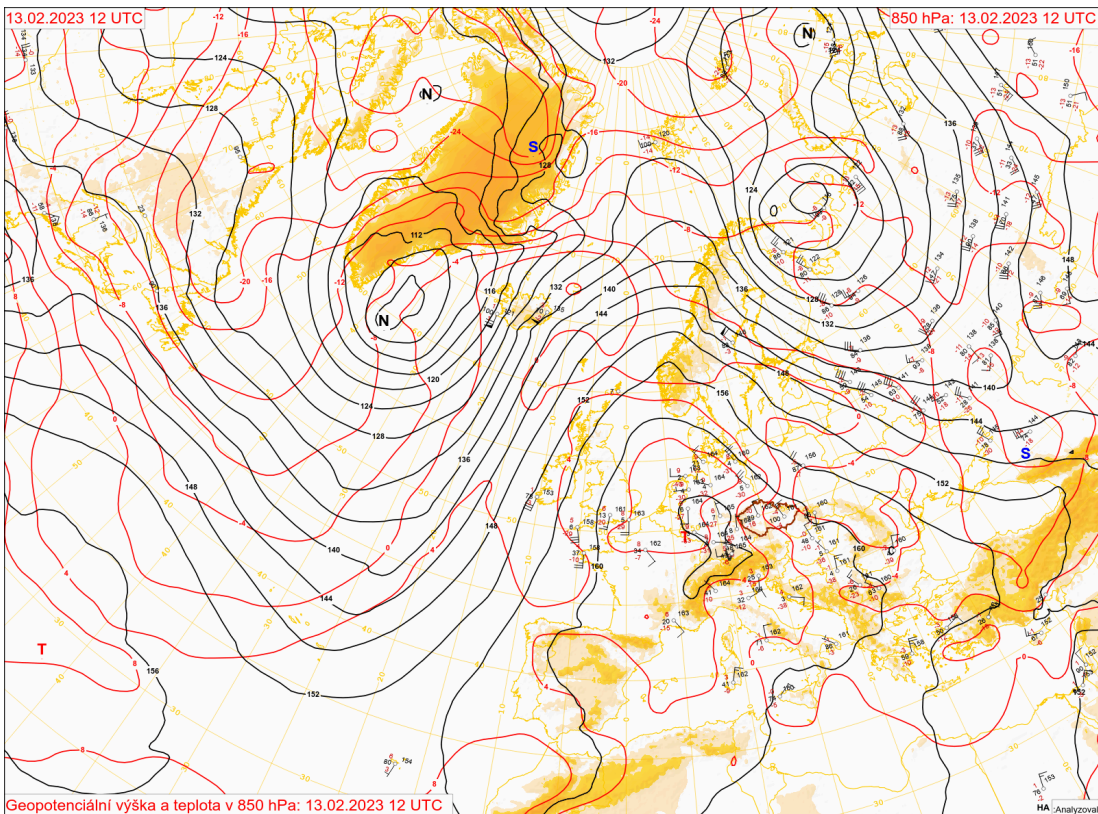
Figure S06: Geopotential height (black) and temperature (red) at 850 hPa for 13 February 2023, 12 UTC. N: cyclone, V: anticyclone. Data source CHMI.

Geopotenciální výška a teplota v 850 hPa: 14.02.2023 00 UTC
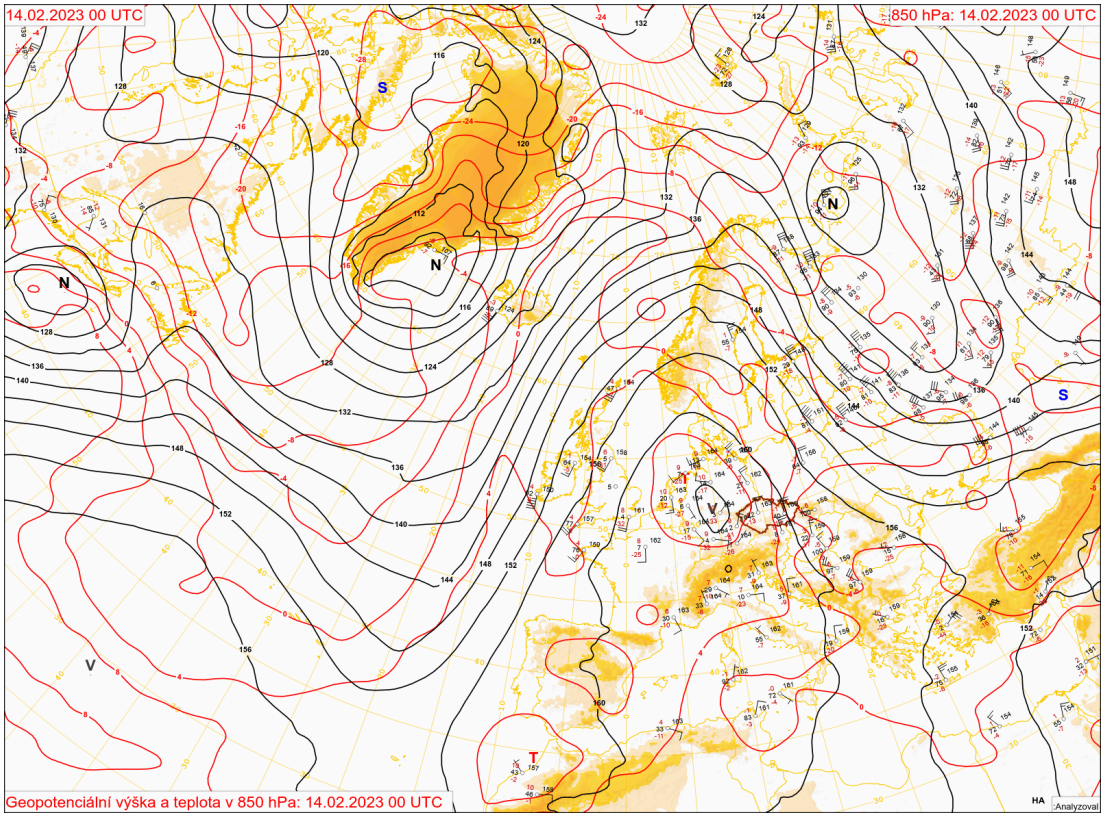
Figure S07: Geopotential height (black) and temperature (red) at 850 hPa for 14 February 2023, 00 UTC. N: cyclone, V: anticyclone. Data source CHMI.

13. 02. 2023: : 18 UTC

SYNOP 13.02.2023 18:0
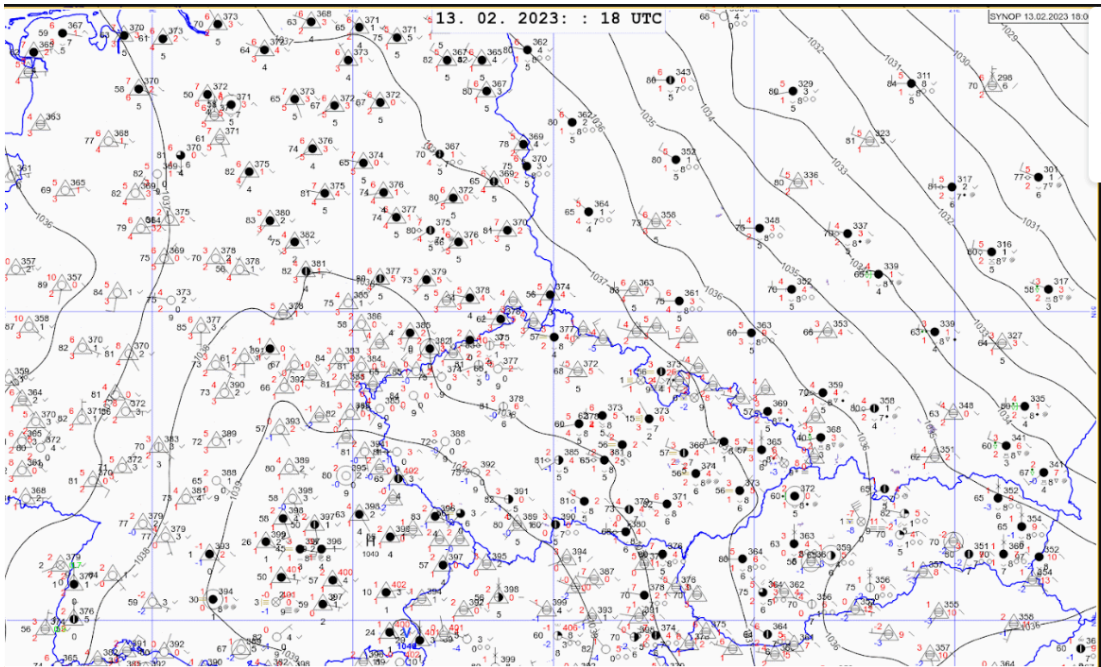
Figure S08: Surface weather analysis with isobars (black) for 13.2. 18:00 UTC ▱ 02 . Data source CHMI.
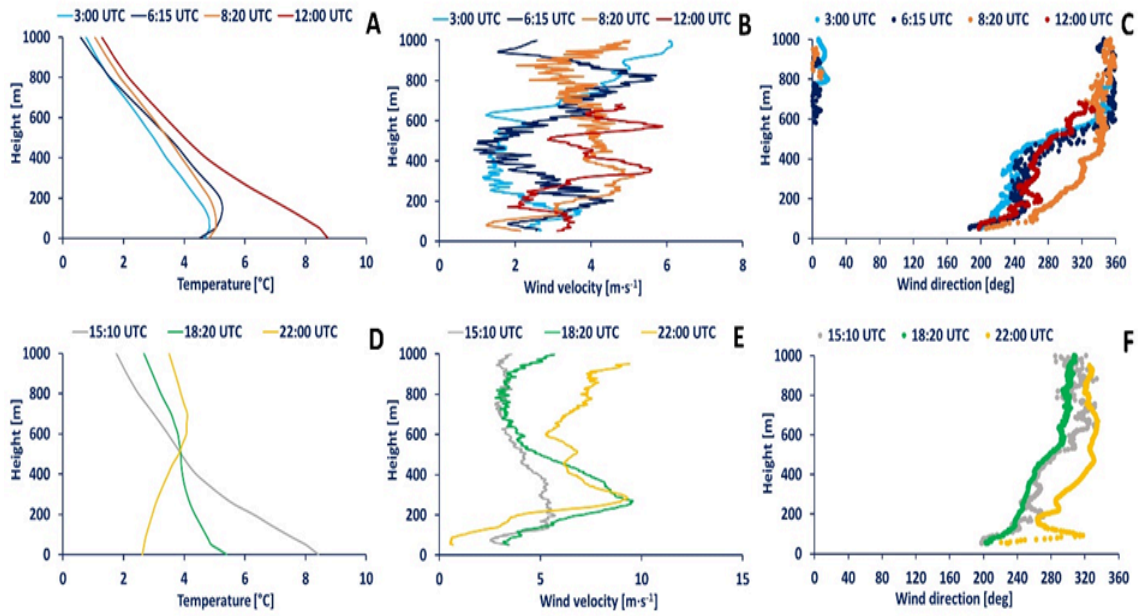
Figure S09: Temperature (A+D), wind velocity (B+E) and wind direction (C+F) profiles measured during 13 February 2023 in Prague TURBAN observation campaign. Change in temperature stratification within the lower boundary layer at selected morning and afternoon hours.
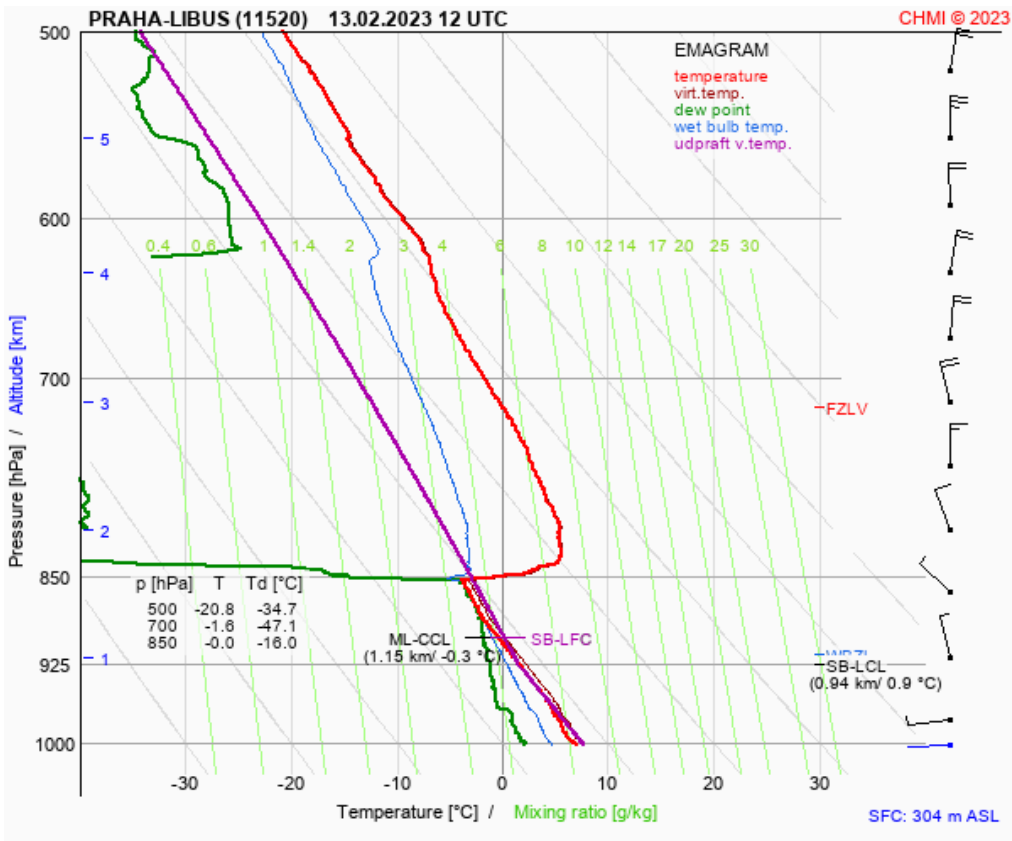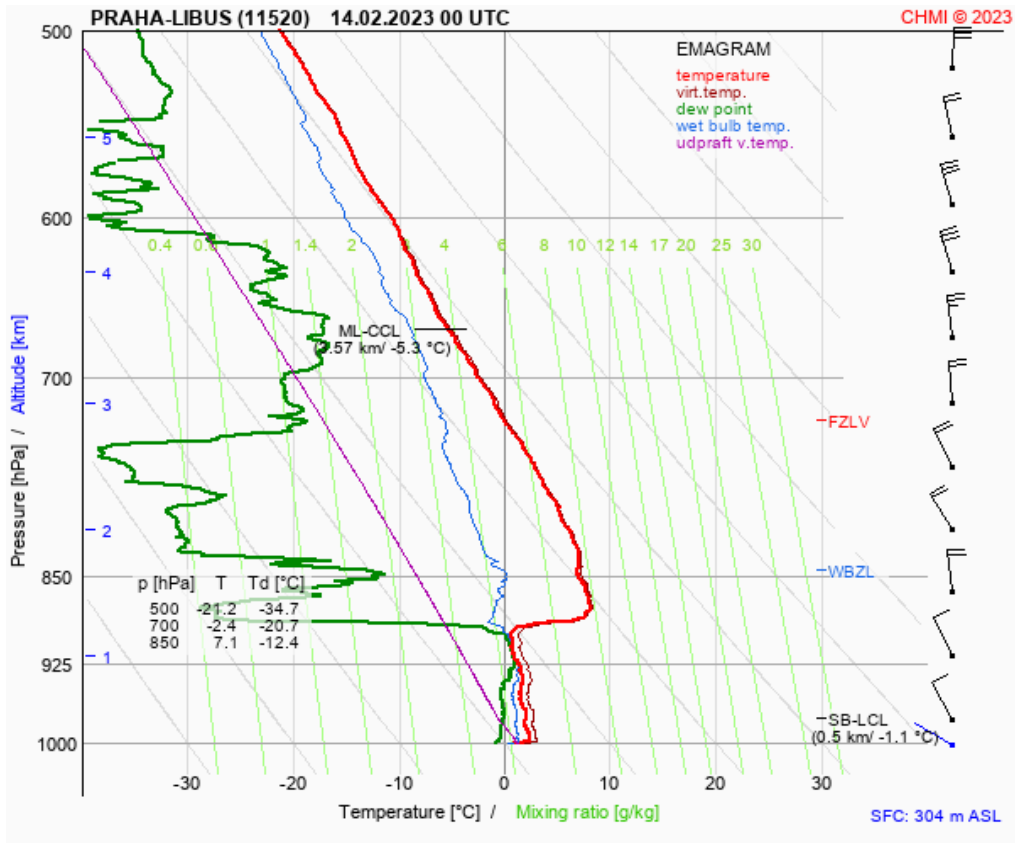
Figure S10: Emagrams from Praha 4-Libuš (WMO ID 11520) soundings *for 13.2. (12h) and 14.2. (00h). Data source CHMI.*

B. Comparison of the ICON, WRF, and ALADIN simulations with soundings in Praha 4-Libuš station

A statistical analysis of the potential temperature, wind speed and direction vertical profiles up to the height of 3000 m a.s.l. and 600 m a.s.l. done for the mesoscale models (ICON, WRF, and ALADIN) against the radio soundings observation obtained from the Praha č-Libuš station (WMO ID 11520): ens. size-ensemble size; mean obs-mean value observations; mean model-mean value from the mesoscale model; RMSE- root mean square error; MBE-mean bias error; r-correlation coefficient. The red color indicates the model with the worst, and the green color indicates the model with the best statistical metrics.

Table S01: Episode 1: 2022-07-17 00:00:00 - 2022-07-20 00:00:00

| WS [m/s]	3000 m a.s.l.			600 m a.s.l.		
	WRF	ICON-D2	ALADIN	WRF	ICON-D2	ALADIN
ens. size	4702	4702	4702	528	528	528
mean. obs.	4.7651	4.7651	4.7651	2.9662	2.9662	2.9662
mean mod.	4.5618	4.4265	4.6367	3.2905	2.2330	3.5765
RMSE	1.5648	1.1938	1.5271	1.4701	1.4924	1.4908
MBE	-0.2033	-0.3387	-0.1285	0.3244	-0.7332	0.6103
r	0.8618	0.9273	0.8688	0.7753	0.8185	0.7813

Theta [K]	3000 m a.s.l.			600 m a.s.l.		
	WRF	ICON-D2	ALADIN	WRF	ICON-D2	ALADIN
ens. size	4702	4702	4702	528	528	528
mean. obs.	299.6530	299.6530	299.6530	295.3264	295.3264	295.3264
mean mod.	299.0824	299.6557	299.5104	294.8280	295.4102	295.8410
RMSE	1.0860	0.4824	0.5852	1.5479	0.8641	1.4350
MBE	-0.5706	0.0026	-0.1426	-0.4984	0.0838	0.5147
r	0.9843	0.9954	0.9936	0.9553	0.9847	0.9627

WDir [deg]	3000 m a.s.l.			600 m a.s.l.		
	WRF	ICON-D2	ALADIN	WRF	ICON-D2	ALADIN
ens. size	4702	4702	4702	528	528	528
mean. obs.	254.0503	254.0503	254.0503	206.5741	206.5741	206.5741
mean mod.	272.3469	257.2193	243.2479	238.1008	210.4253	220.9560

RMSE	77.2417	72.6730	76.1917	78.9306	76.2414	79.3055
MBE	18.2965	3.1689	-10.8024	31.5266	3.8512	14.3819
r	0.6846	0.7321	0.7208	0.6366	0.6135	0.5507

Table S02: Episode 2: 2022-08-02 00:00:00 - 2022-08-06 00:00:00

WS [m/s]	3000 m a.s.l.			600 m a.s.l.		
	WRF	ICON-D2	ALADIN	WRF	ICON-D2	ALADIN
ens. size	6501	6501	6501	705	705	705
mean. obs.	4.0226	4.0226	4.0226	4.1031	4.1031	4.1031
mean mod.	4.3123	3.8524	4.1102	4.6606	3.3987	4.6126
RMSE	1.9221	1.1284	1.4996	1.9611	1.7292	1.9523
MBE	0.2897	-0.1701	0.0877	0.5575	-0.7044	0.5095
r	0.7614	0.8973	0.8081	0.8646	0.9285	0.8466

Theta [K]	3000 m a.s.l.			600 m a.s.l.		
	WRF	ICON-D2	ALADIN	WRF	ICON-D2	ALADIN
ens. size	6501	6501	6501	705	705	705
mean. obs.	303.1334	303.1331	303.1331	299.4092	299.4092	299.4092
mean mod.	302.8559	303.0261	303.0516	298.9366	299.2119	299.8093
RMSE	1.1740	0.6446	0.5684	1.4205	1.1922	1.0722
MBE	-0.2772	-0.1070	-0.0815	-0.4727	-0.1974	0.4000
r	0.9634	0.9865	0.9888	0.9455	0.9590	0.9686

W.Dir. [deg]	3000 m a.s.l.			600 m a.s.l.		
	WRF	ICON-D2	ALADIN	WRF	ICON-D2	ALADIN
ens. size	6501	6501	6501	705	705	705
mean. obs.	199.7091	199.7091	199.7091	184.3922	184.3922	184.3922
mean mod.	206.9160	205.5264	196.2261	166.6572	201.6190	183.6304
RMSE	99.8123	65.0311	79.3272	130.4314	79.4885	76.0843
MBE	7.2069	5.8173	-3.4830	-17.7350	17.2268	-0.7618

| r | 0.4050 | 0.7507 | 0.6418 | -0.2108 | 0.4464 | 0.5118 |

Table S03: Episode 3: 2022-09-22 00:00:00 - 2022-09-25 00:00:00

WS [m/s]	3000 m a.s.l.			600 m a.s.l.		
	WRF	ICON-D2	ALADIN	WRF	ICON-D2	ALADIN
ens. size	5050	5050	5050	583	583	583
mean. obs.	3.2452	3.2452	3.2452	2.6676	2.6676	2.6676
mean mod.	3.2528	2.9664	3.1579	2.6968	2.1730	3.2669
RMSE	1.4383	1.1314	1.3106	1.9721	1.5134	1.5881
MBE	0.0076	-0.2789	-0.0873	0.0292	-0.4947	0.5993
r	0.6872	0.8042	0.7261	0.4873	0.5451	0.5945

Theta [K]	3000 m a.s.l.			600 m a.s.l.		
	WRF	ICON-D2	ALADIN	WRF	ICON-D2	ALADIN
ens. size	5050	5050	5050	583	583	583
mean. obs.	290.9965	290.9965	290.9965	286.0544	286.0544	286.0544
mean mod.	290.8566	290.9516	290.8174	285.5889	286.0260	286.4246
RMSE	0.9740	0.5555	0.6354	1.0696	0.5652	0.9085
MBE	-0.1398	-0.0449	-0.1791	-0.4655	-0.0284	0.3702
r	0.9764	0.9921	0.9903	0.9408	0.9808	0.9761

W.Dir. [deg]	3000 m a.s.l.			600 m a.s.l.		
	WRF	ICON-D2	ALADIN	WRF	ICON-D2	ALADIN
ens. size	5050	5050	5050	583	583	583
mean. obs.	239.2448	239.2448	239.2448	215.1145	215.1145	215.1145
mean mod.	224.9361	232.2341	225.2463	223.6745	218.4773	201.3437
RMSE	119.9099	100.5258	118.7961	63.1580	75.1142	115.4956
MBE	-14.3085	-7.0107	-13.9985	8.5600	3.3628	-13.7708
r	0.2857	0.4488	0.2838	0.6660	0.4747	0.0136

Table S04: Episode4: 2022-10-10 00:00:00 - 2022-10-15 00:00:00

WS [m/s]	3000 m a.s.l.			600 m a.s.l.		
	WRF	ICON-D2	ALADIN	WRF	ICON-D2	ALADIN
ens. size	7604	7604	7604	898	898	898
mean. obs.	5.9318	5.9318	5.9318	4.1234	4.1234	4.1234
mean mod.	6.0487	5.7665	5.8493	4.9175	3.6723	4.7982
RMSE	2.0561	1.2328	1.6524	2.7987	1.1319	1.6814
MBE	0.1169	-0.1653	-0.0825	0.7942	-0.4511	0.6748
r	0.7355	0.9071	0.8226	0.6183	0.9070	0.7827

Theta [K]	3000 m a.s.l.			600 m a.s.l.		
	WRF	ICON-D2	ALADIN	WRF	ICON-D2	ALADIN
ens. size	7604	7604	7604	898	898	898
mean. obs.	293.2012	293.2012	293.2012	286.4834	286.4834	286.4834
mean mod.	293.0572	293.1638	292.9616	286.4235	286.4282	286.8911
RMSE	1.0476	0.5431	0.8456	1.5962	0.7347	1.2013
MBE	-0.1440	-0.0374	-0.2396	-0.0599	-0.0552	0.4077
r	0.9781	0.9941	0.9868	0.8361	0.9611	0.8737

W.Dir. [deg]	3000 m a.s.l.			600 m a.s.l.		
	WRF	ICON-D2	ALADIN	WRF	ICON-D2	ALADIN
ens. size	7604	7604	7604	898	898	898
mean. obs.	225.6659	225.6659	225.6659	168.3376	168.3376	168.3376
mean mod.	225.0100	227.9061	222.1888	163.2312	173.1999	158.9250
RMSE	57.0364	41.6589	56.2491	92.6477	25.7007	90.2430
MBE	-0.6549	2.2402	-3.4771	-5.1064	4.8623	-9.4126
r	0.6203	0.7988	0.6571	0.3878	0.9556	0.4036

Table S05: Episode 5: 2022-11-27 00:00:00 - 2022-11-30 12:00:00

WS [m/s]	3000 m a.s.l.			600 m a.s.l.		
	WRF	ICON-D2	ALADIN	WRF	ICON-D2	ALADIN
ens. size	5698	5698	5698	659	659	659
mean. obs.	4.1417	4.1417	4.1417	3.5980	3.5980	3.5980
mean mod.	4.1022	4.0799	4.0740	4.4164	3.8289	3.9006
RMSE	1.8620	1.2433	1.2434	2.2258	1.0855	1.5044
MBE	-0.0395	-0.0617	-0.0677	0.8183	0.2308	0.3026
r	0.6474	0.8032	0.7958	0.5626	0.7652	0.5182

Theta [K]	3000 m a.s.l.			600 m a.s.l.		
	WRF	ICON-D2	ALADIN	WRF	ICON-D2	ALADIN
ens. size	5698	5698	5698	659	659	659
mean. obs.	285.5034	285.5034	285.5034	277.6396	277.6396	277.6396
mean mod.	285.3230	285.4798	285.3024	277.5965	277.5756	277.7103
RMSE	1.2150	0.6248	0.8696	1.4448	0.7415	0.9647
MBE	-0.1804	-0.0236	-0.2010	-0.0431	-0.0640	0.0707
r	0.9761	0.9936	0.9882	0.4877	0.8791	0.7860

W.Dir. [deg]	3000 m a.s.l.			600 m a.s.l.		
	WRF	ICON-D2	ALADIN	WRF	ICON-D2	ALADIN
ens. size	5698	5698	5698	659	659	659
mean. obs.	203.8924	203.8924	203.8924	158.5479	158.5479	158.5479
mean mod.	196.9039	204.3398	207.9014	167.0591	161.3301	168.2070
RMSE	53.1001	27.1723	32.9289	26.8072	25.8049	18.4697
MBE	-6.9885	0.4474	4.0090	8.5112	2.7822	9.6591
r	0.7315	0.9324	0.9006	0.8441	0.8437	0.9433

Table S06: Episode 6: 2022-12-08 06:00:00 - 2022-12-11 00:00:00

WS [m/s]	3000 m a.s.l.			600 m a.s.l.		
	WRF	ICON-D2	ALADIN	WRF	ICON-D2	ALADIN
ens. size	4321	4321	4321	471	471	471
mean. obs.	6.5390	6.5390	6.5390	3.6468	3.6468	3.6468
mean mod.	6.3904	6.4478	6.1261	4.4276	3.7712	4.6355
RMSE	2.6810	1.2708	1.8407	1.5363	1.2743	1.5936
MBE	-0.1486	-0.0912	-0.4129	0.7807	0.1244	0.9887
r	0.7005	0.9361	0.8665	0.8047	0.8735	0.8457

Theta [K]	3000 m a.s.l.			600 m a.s.l.		
	WRF	ICON-D2	ALADIN	WRF	ICON-D2	ALADIN
ens. size	4321	4321	4321	471	471	471
mean. obs.	282.0536	282.0536	282.0536	276.7705	276.7705	276.7705
mean mod.	281.8283	282.0577	282.0838	276.1946	276.4533	276.4782
RMSE	1.2230	0.6644	0.7964	1.0363	0.5961	0.5715
MBE	-0.2253	0.0041	0.0302	-0.5759	-0.3172	-0.2923
r	0.9665	0.9897	0.9851	0.7778	0.9279	0.9320

W.Dir. [deg]	3000 m a.s.l.			600 m a.s.l.		
	WRF	ICON-D2	ALADIN	WRF	ICON-D2	ALADIN
ens. size	4321	4321	4321	471	471	471
mean. obs.	226.5675	226.5675	226.5675	191.2169	191.2169	191.2169
mean mod.	213.3720	224.6504	218.2561	161.7442	215.6880	187.7843
RMSE	76.3537	57.4781	79.7380	127.3560	80.1106	88.6946
MBE	-13.1955	-1.9170	-8.3114	-29.4726	24.4712	-3.4326
r	0.6178	0.7658	0.5912	0.4570	0.7882	0.7244

Table S07: Episode 7: 2023-01-22 00:00:00 - 2023-01-30 00:00:00

WS [m/s]	3000 m a.s.l.			600 m a.s.l.		
	WRF	ICON-D2	ALADIN	WRF	ICON-D2	ALADIN
ens. size	12224	12224	12224	1347	1347	1347
mean. obs.	7.0544	7.0544	7.0544	3.6636	3.6636	3.6636
mean mod.	6.9973	6.9184	6.9076	4.0836	3.8957	4.3709
RMSE	1.7603	1.2964	1.4696	2.1234	1.0924	1.5506
MBE	-0.0571	-0.1360	-0.1468	0.4201	0.2321	0.7073
r	0.8738	0.9338	0.9122	0.6921	0.9056	0.8490

Theta [K]	3000 m a.s.l.			600 m a.s.l.		
	WRF	ICON-D2	ALADIN	WRF	ICON-D2	ALADIN
ens. size	12224	12224	12224	1347	1347	1347
mean. obs.	282.7323	282.7323	282.7323	273.4727	273.4727	273.4727
mean mod.	282.5831	282.7340	282.8216	273.0310	273.3957	273.2551
RMSE	1.1342	0.8209	1.0829	1.0349	0.2920	0.6145
MBE	-0.1493	0.0017	0.0893	-0.4418	-0.0770	-0.2176
r	0.9832	0.9934	0.9886	0.7363	0.9792	0.9098

W.Dir. [deg]	3000 m a.s.l.			600 m a.s.l.		
	WRF	ICON-D2	ALADIN	WRF	ICON-D2	ALADIN
ens. size	12224	12224	12224	1347	1347	1347
mean. obs.	116.8070	116.8070	116.8070	145.4419	145.4419	145.4419
mean mod.	105.6133	112.4370	104.1647	123.2024	156.9203	89.5693
RMSE	76.5071	71.8640	73.5836	123.8994	147.8780	141.8466
MBE	-11.1937	-4.3700	-12.6423	-22.2395	11.4784	-55.8726
r	0.6986	0.7498	0.7229	0.5433	0.3984	0.3894

Table S08: Episode 8: 2023-02-06 00:00:00 - 2023-02-11 00:00:00

WS [m/s]	3000 m a.s.l.			600 m a.s.l.		
	WRF	ICON-D2	ALADIN	WRF	ICON-D2	ALADIN
ens. size	8310	8310	8310	911	911	911
mean. obs.	6.9023	6.9023	6.9023	3.3635	3.3635	3.3635
mean mod.	6.9073	6.9620	6.8012	5.1216	3.5252	4.3041
RMSE	2.2876	1.4125	1.6055	3.5220	1.0795	1.8378
MBE	0.0050	0.0598	-0.1010	1.7581	0.1617	0.9406
r	0.7915	0.9232	0.8983	0.7187	0.9192	0.8385

Theta [K]	3000 m a.s.l.			600 m a.s.l.		
	WRF	ICON-D2	ALADIN	WRF	ICON-D2	ALADIN
ens. size	8310	8310	8310	911	911	911
mean. obs.	280.1616	280.1616	280.1616	271.0146	271.0146	271.0146
mean mod.	279.7813	280.1090	279.9262	271.3481	270.6315	271.4839
RMSE	1.1334	0.7351	0.8374	1.0307	0.8761	1.0785
MBE	-0.3803	-0.0526	-0.2354	0.3335	-0.3831	0.4693
r	0.9882	0.9942	0.9927	0.9039	0.9453	0.9050

W.Dir. [deg]	3000 m a.s.l.			600 m a.s.l.		
	WRF	ICON-D2	ALADIN	WRF	ICON-D2	ALADIN
ens. size	8310	8310	8310	911	911	911
mean. obs.	158.6581	158.6581	158.6581	178.0343	178.0343	178.0343
mean mod.	154.2268	156.5691	162.8395	172.2907	163.8846	202.1606
RMSE	60.7553	52.4265	54.4268	96.9434	97.9929	75.1761
MBE	-4.4313	-2.0890	4.1814	-5.7436	-14.1497	24.1263
r	0.8316	0.8772	0.8840	0.2895	0.3229	0.6185

Table S09: Episode 9: 2023-02-13 00:00:00 - 2023-02-16 00:00:00

WS [m/s]	3000 m a.s.l.			600 m a.s.l.		
	WRF	ICON-D2	ALADIN	WRF	ICON-D2	ALADIN
ens. size	5240	5240	5240	572	572	572
mean. obs.	5.5750	5.5750	5.5750	2.2548	2.2548	2.2548
mean mod.	5.8333	5.4547	5.6748	2.8292	2.6335	2.8703
RMSE	1.7576	1.2086	1.4170	2.6460	1.2547	2.0063
MBE	0.2583	-0.1203	0.0998	0.5744	0.3786	0.6155
r	0.8436	0.9268	0.8966	0.1770	0.6188	0.2809

Theta [K]	3000 m a.s.l.			600 m a.s.l.		
	WRF	ICON-D2	ALADIN	WRF	ICON-D2	ALADIN
ens. size	5240	5240	5240	572	572	572
mean. obs.	290.1704	290.1704	290.1704	276.3340	276.3340	276.3340
mean mod.	290.2200	290.2321	290.8033	277.7849	276.4161	277.9397
RMSE	2.1525	0.7033	1.8160	3.9958	0.6092	2.6984
MBE	0.0496	0.0617	0.6329	1.4509	0.0821	1.6057
r	0.9723	0.9967	0.9830	-0.3726	0.9733	0.5927

W.Dir. [deg]	3000 m a.s.l.			600 m a.s.l.		
	WRF	ICON-D2	ALADIN	WRF	ICON-D2	ALADIN
ens. size	5240	5240	5240	572	572	572
mean. obs.	244.5890	244.5890	244.5890	222.6436	222.6436	222.6436
mean mod.	257.2488	241.1400	266.6472	214.9036	207.3581	237.7551
RMSE	169.1670	151.9895	145.5366	112.7940	117.4503	103.3530
MBE	12.6598	-3.4490	22.0582	-7.7400	-15.2855	15.1115
r	0.0203	0.2755	0.2447	-0.1417	-0.3610	-0.0977

C. Comparison of the ICON, WRF, and ALADIN simulations with with LIDAR and Microwave observations

A statistical analysis of the potential temperature, wind speed, and wind direction vertical profiles done for the mesoscale models (ICON, WRF, and ALADIN) against the LIDAR and MW observations gathered during the observation campaign for Episode 9: ens. size-ensemble size; mean obs.-mean value observations; mean mod.-mean value from the mesoscale model; RMSE- root mean square error; MBE-mean bias error; r-correlation coefficient. The red color indicates the model with the worst, and the green color indicates the model with the best statistical metrics out of the three.

Table S10: Episode 9: 2023-02-13 00:00:00 - 2023-02-16 00:00:00

WS [m/s]	snr >= 1.015; 1700 m a.s.l.		
	WRF	ICON-D2	ALADIN
ens. size	15497	15497	15497
mean. obs.	3.4517	3.4517	3.4517
mean mod.	3.4358	2.6879	3.0232
RMSE	2.6689	2.4505	2.2059
MBE	-0.0159	-0.7638	-0.4285
r	0.3515	0.4106	0.5339

Theta [K]	1261 m a.s.l.		
	WRF	ICON-D2	ALADIN
ens. size	1606	1606	1606
mean. obs.	279.8331	279.8331	279.8331
mean mod.	280.8903	279.9068	280.7523
RMSE	2.9268	1.8301	2.0779
MBE	1.0572	0.0737	0.9192
r	0.7859	0.9259	0.9026

Temp [deg]	1261 m a.s.l.		
	WRF	ICON-D2	ALADIN
ens. size	1606	1606	1606
mean. obs.	3.0442	3.0442	3.0442
mean mod.	3.6779	2.6708	3.4216

RMSE	2.5896	1.7501	1.7325
MBE	0.6337	0.3734	0.3774
r	0.3767	0.8389	0.7480

W.Dir. [deg]	snr >= 1.015; 1700 m a.s.l.		
	WRF	ICON-D2	ALADIN
ens. size	15497	15497	15497
mean. obs.	223.5329	223.5329	223.5329
mean mod.	227.1142	228.5869	248.6291
RMSE	87.3645	103.3606	83.7829
MBE	3.5812	5.0529	25.0961
r	0.5088	0.2981	0.5268

D. Comparison of the wind speed, wind direction, and potential temperature profiles modeled by mesoscale models with LIDAR and MW observations

Lidar vs dynamic drivers — wind speed and wind direction profiles for 2023-02-13, hourly panels from 07:00 to 15:00, comparing ALAD, ICON, WRF and Lidar.
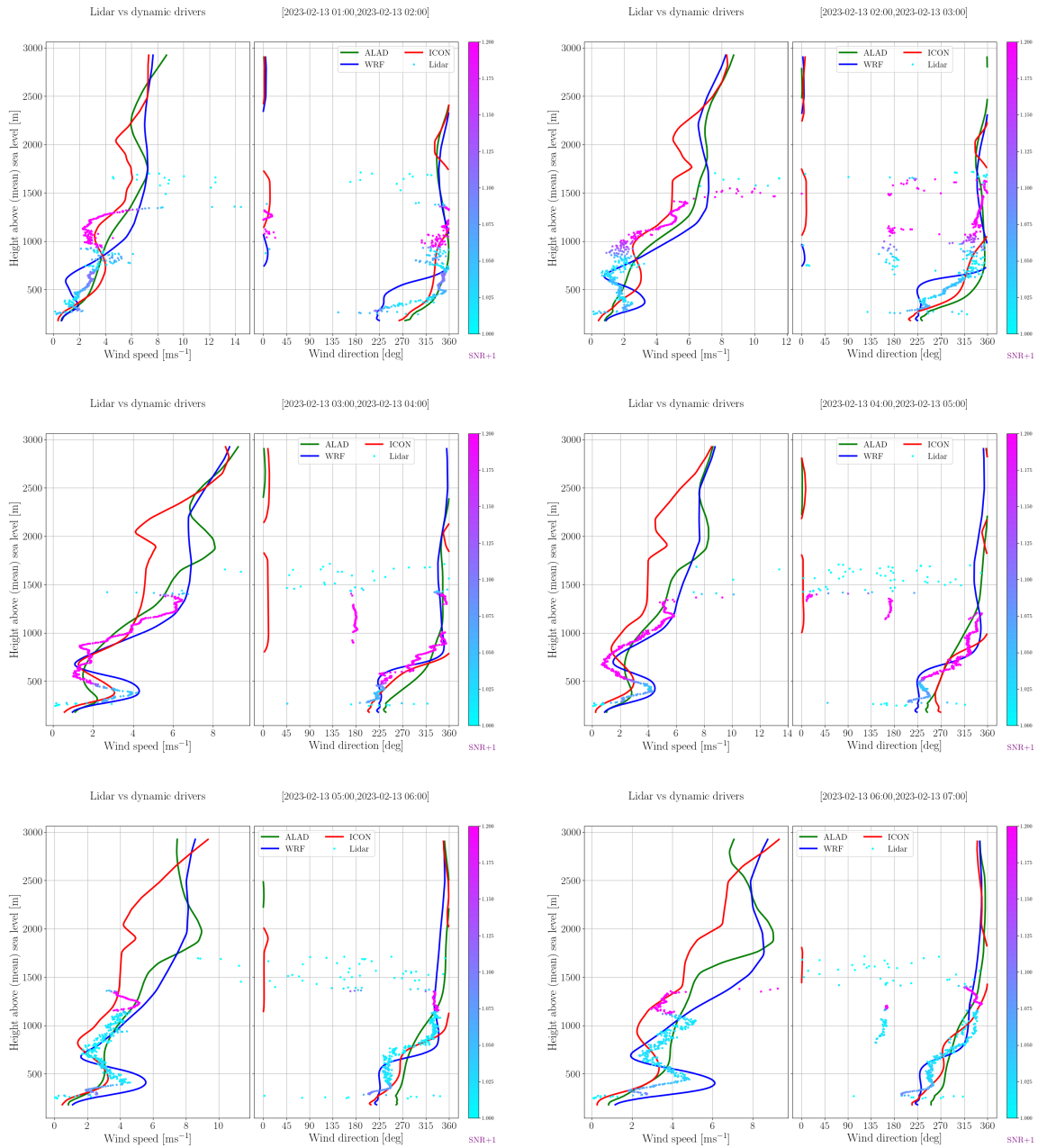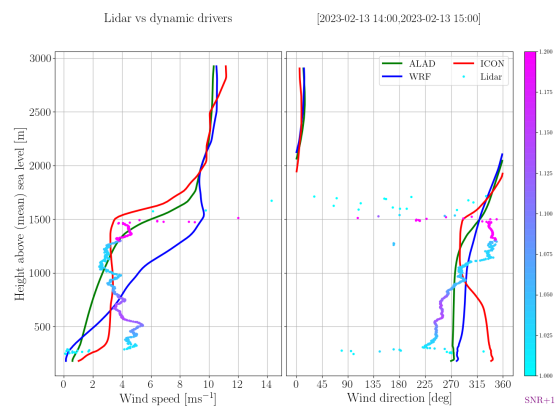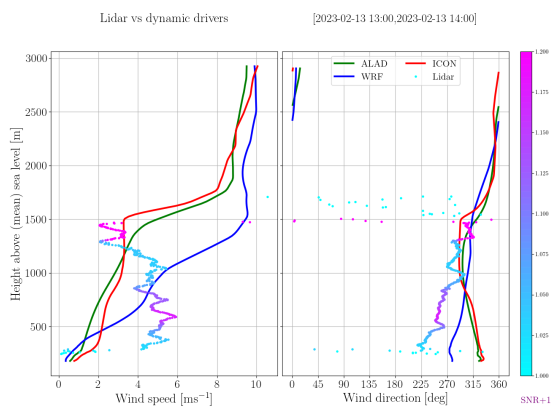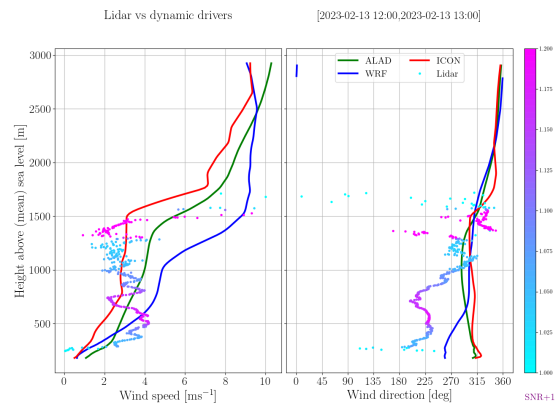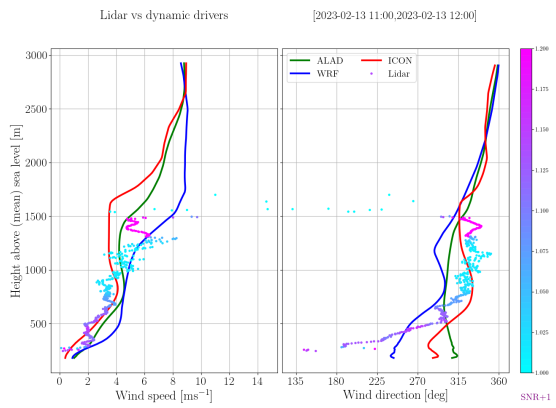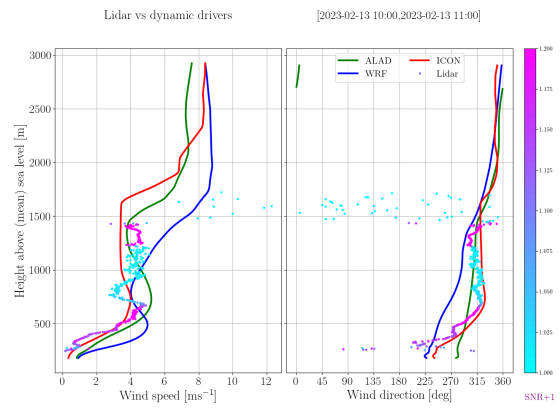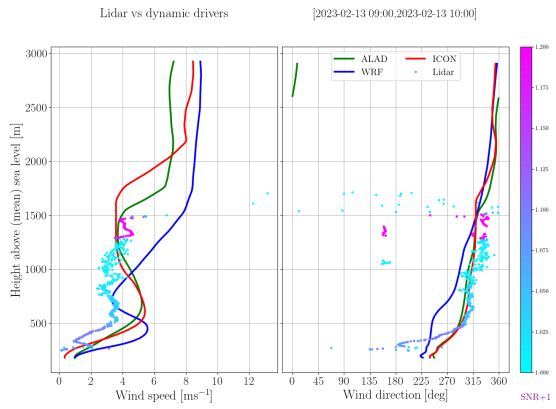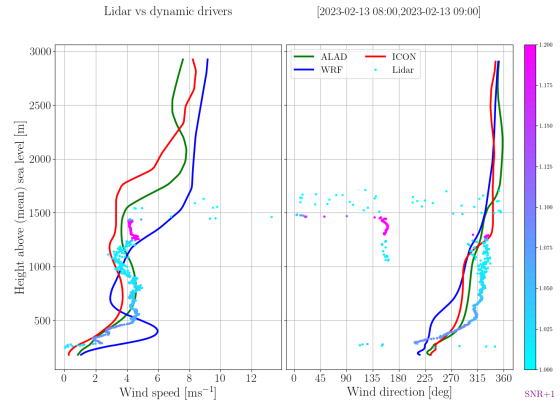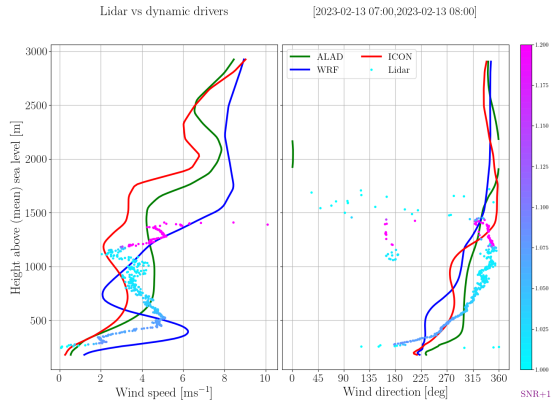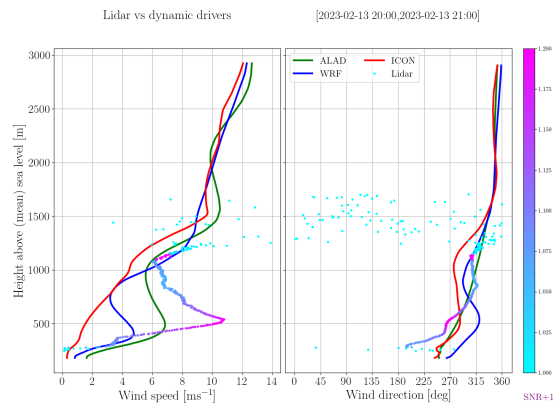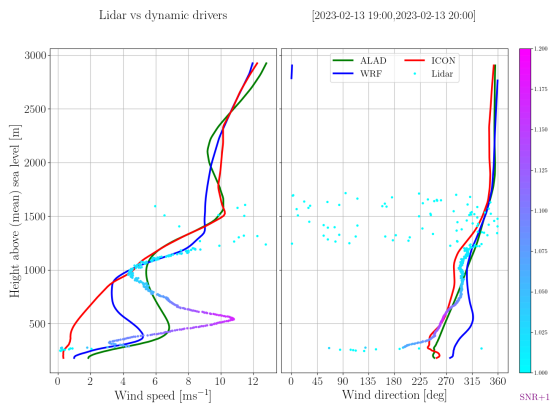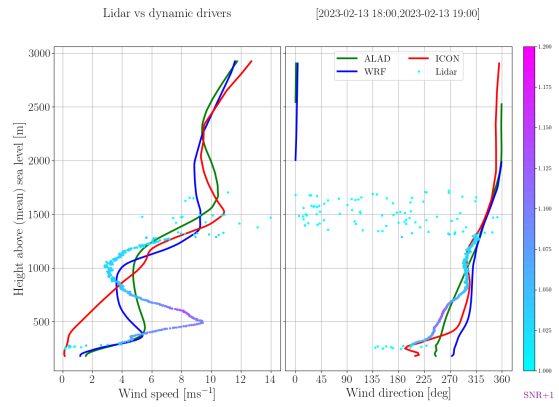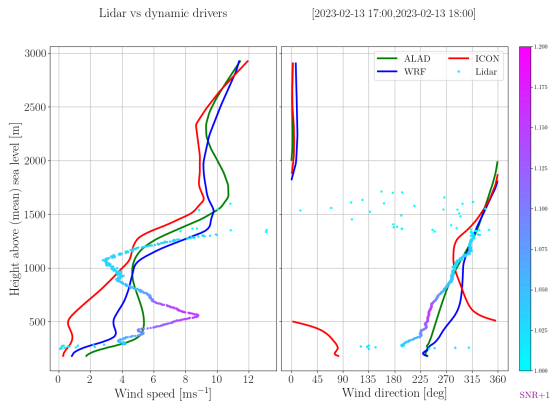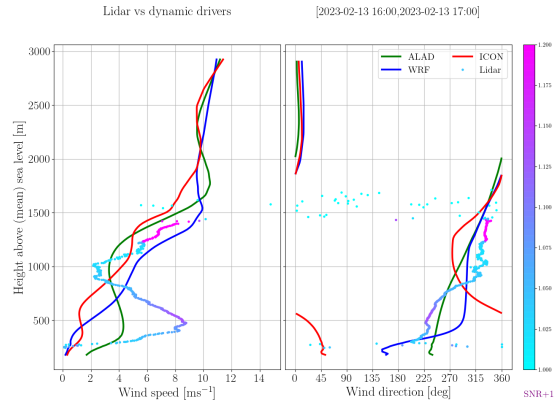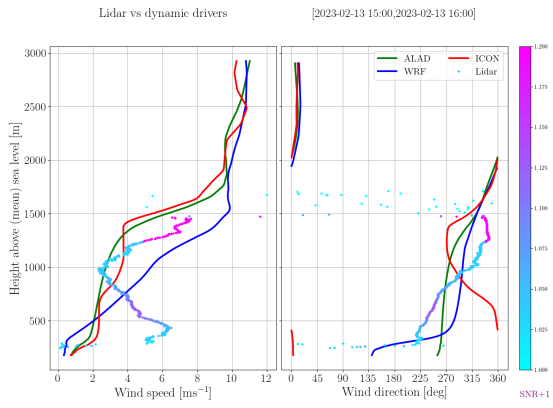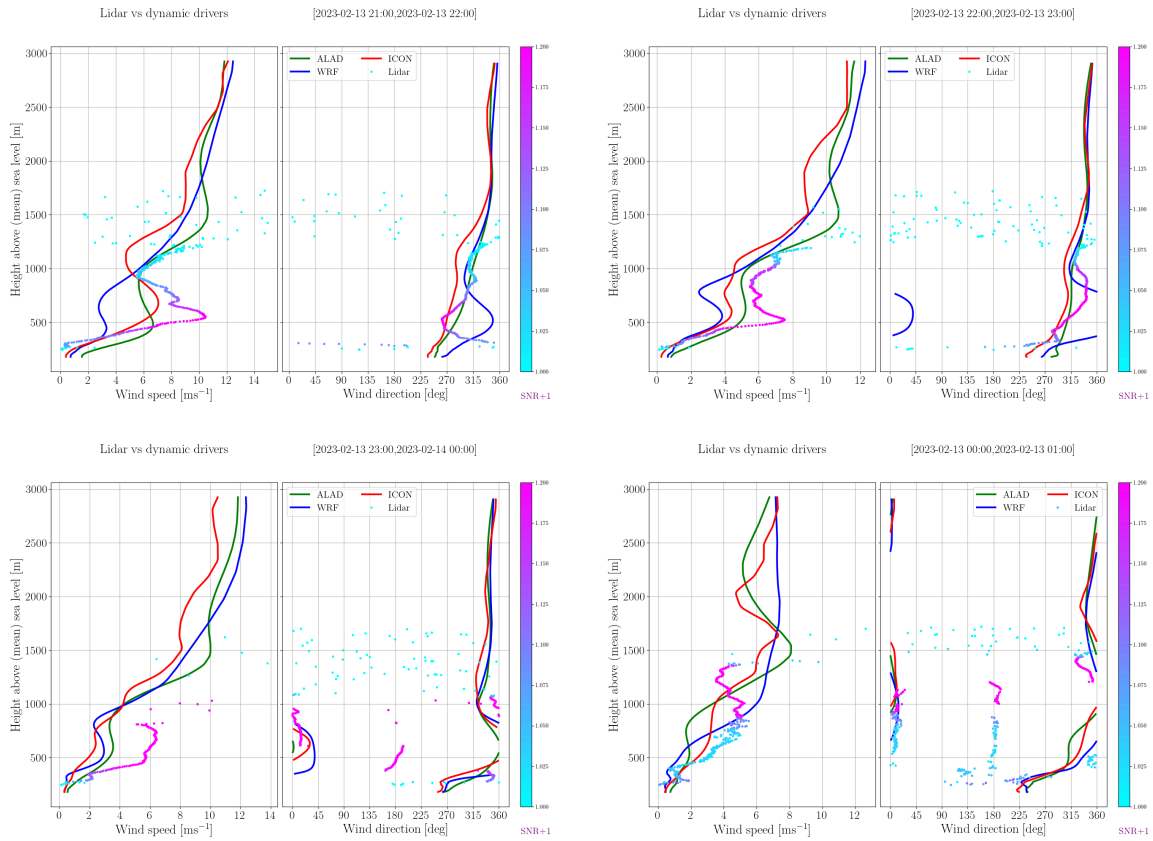
Fig. S11: Comparison of the wind speed and wind direction profiles modeled by mesoscale models ICON (red), ALADIN (green), and WRF (blue) used as PALM model BC with profiles from LIDAR observations for 13.2.2023. The color of the LIDAR observation dotted line shows the LIDAR signal/noise ratio and the uncertainty of the observation.
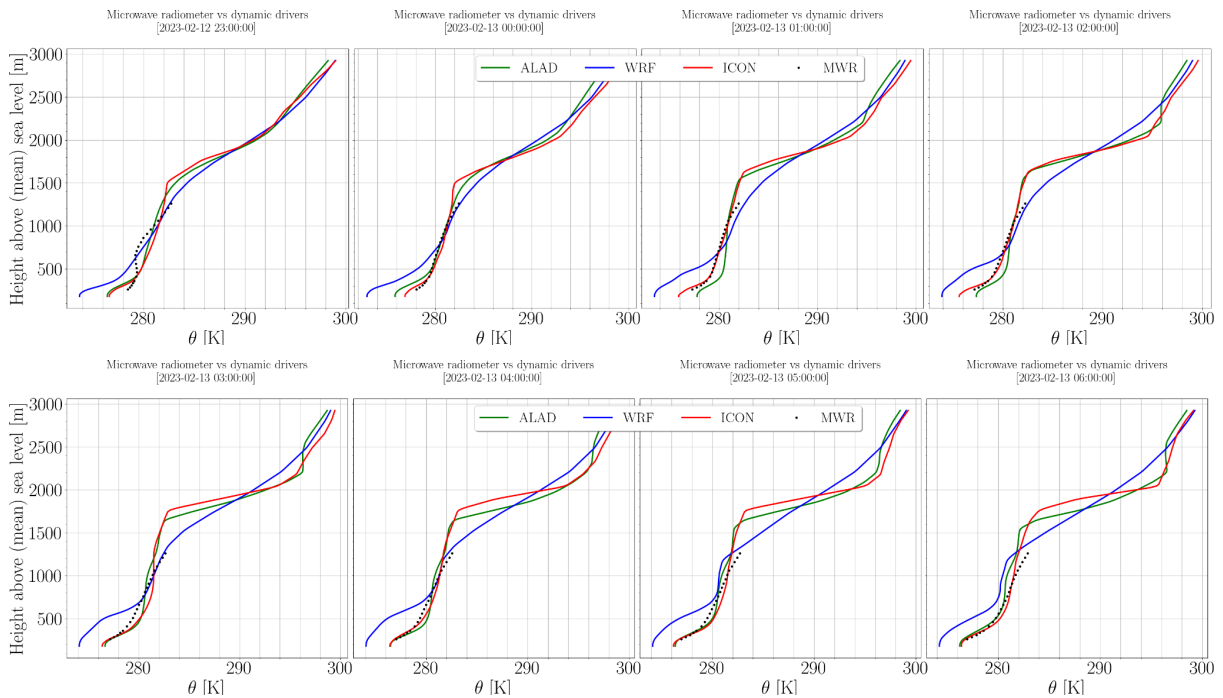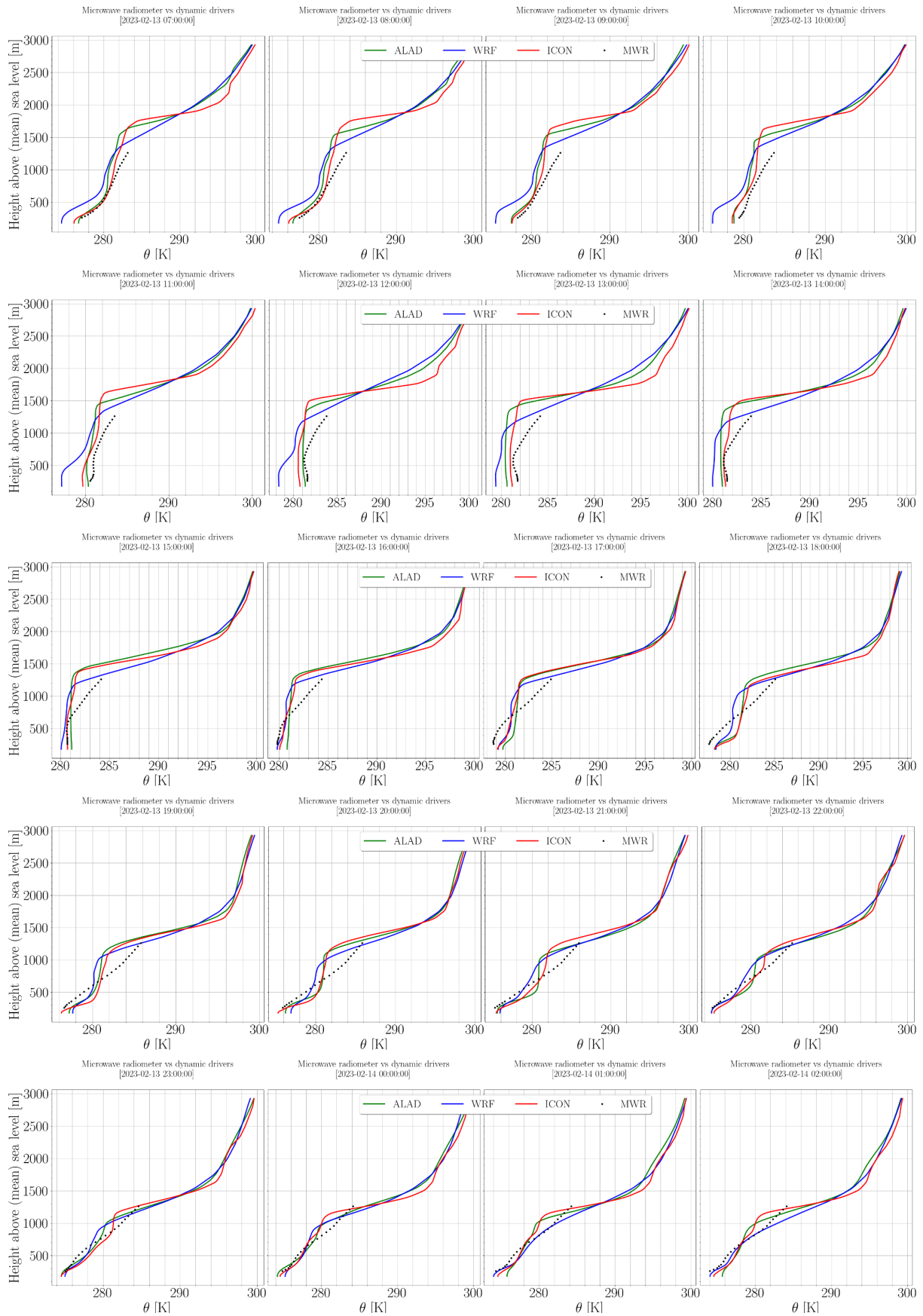
Fig. S12: Comparison of the potential temperature profiles modeled by mesoscale models ICON (red), ALADIN (green), and WRF (blue) used as PALM model BC with profiles from MW observations for 13.2.2023.

E. Air quality sensor network
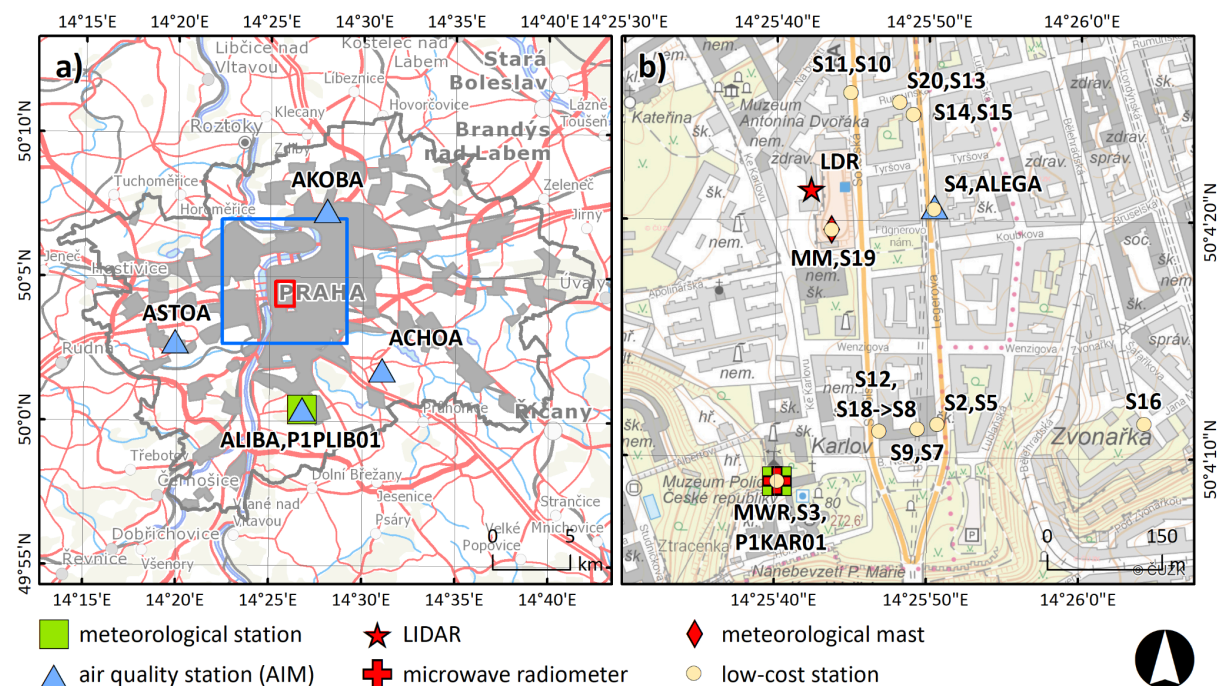
Fig. S13: Locations of air quality stations used for the construction of boundary conditions and Praha 4-Libuš used for profile validation (a). Measurement locations in Legerova street and its surroundings (b) of individual low-cost sensors for air quality monitoring (stations with S prefix) and supplementary meteorological measurements. If there is a pair of sensors in one location, the lower one is listed first. Detailed information about locations and abbreviations used in this figure are explained in Table S11. Background data in (a) is a WMS service with ArcČR layer (https://www.arcdata.cz/cs-cz/produkty/data/arccr), topographical map in (b) is web map service of the Czech Office for Surveying, Mapping and Cadastre – ČÚZK.

Table S11: List of all measurements used for the TURBAN project with the locations metadata. Coordinates are given in decimal degrees. Station classification follows the classification method used in the air quality RM network (CHMI, Czech Republic). Air quality low-cost sensors (LCSs) placed in higher height (within pairs) are underlined in blue, LCSs collocated with reference monitors (RM) are underlined in gray.

Station name	Station ID	Final deployment location name	Latitude	Longitude	Ground elevation (m ASL)	Height (m AGL)	Station classification*	Measurement start date
AQ Sensor 2	S2	school Legerova (lower height)	50.069833	14.43075	237	5.8	T	30/05/2022
AQ Sensor 5	S5	school Legerova (higher height)	50.069833	14.43075	237	13.2	T	30/05/2022
AQ Sensor 9	S9	School courtyard (lower height)	50.069778	14.430389	237	4.7	UB	31/05/2022
AQ Sensor 7	S7	School courtyard (higher height)	50.069778	14.430389	237	6.9	UB	31/05/2022
AQ Sensor 12	S12	school Sokolská (lower height)	50.06975	14.429694	236	5.9	T	30/05/2022
AQ Sensor 18	S18	school Sokolská (higher height)	50.06975	14.429694	236	13.1	T	30/05/2022
AQ Sensor 8	S8	RM Libuš	50.0073	14.44593	301	2.5	SUB	22/05/2022
		school Sokolská (higher height)	50.06975	14.429694	236	13.1	UB	15/02/2023
AQ Sensor 14	S14	Legerova (lower height)	50.073472	14.430278	236	9.2	T	30/05/2022
AQ Sensor 15	S15	Legerova (higher height)	50.073472	14.430278	236	14.6	T	30/05/2022
AQ Sensor 20	S20	Rumunská (lower height)	50.073611	14.430028	236	4.6	T	30/05/2022
AQ Sensor 13	S13	Rumunská (higher height)	50.073611	14.430028	236	14.8	T	30/05/2022
AQ Sensor 11	S11	CKAIT Sokolská (lower height)	50.073722	14.429139	235	5.5	T	30/05/2022
AQ Sensor 10	S10	CKAIT Sokolská (higher height)	50.073722	14.429139	235	12.2	T	31/05/2022

AQ Sensor 19	**S19**	PVK garden (on meteo-mast)	50.072111	14.428806	241	2.6	U	01/06/2022
AQ Sensor 3	**S3**	MS Karlov (roof)	50.069157	14.427839	235	30	UB	23/02/2022
AQ Sensor 16	**S16**	Hotel Le Palais Art Prague (roof)	50.069854	14.434532	238	22	UB	19/07/2022
AQ Sensor 4	**S4**	RM Legerova	50.072361	14.430667	238	2.1	T (hotspot)	24/03/2022
AQ Sensor 6	**S6**	RM Libuš	50.007305	14.445933	301	2.5	SUB	16/12/2021
AQ Sensor 17	**S17**	RM Libuš	50.007305	14.445933	301	2.5	SUB	16/12/2021
Doppler LIDAR	**LDR**	PVK roof	50.072588	14.428428	235	4.5	U	24/03/2022
Microwave radiometer	**MWR**	MS Karlov roof**	50.069157	14.427839	235	29.5	UB	23/02/2022
Meteo-mast PVK	**MM**	PVK garden	50.072111	14.428806	241	7.5***	U	01/06/2022
AQM Praha 2 - Legerova	**ALEGA**	RM Legerova	50.072388	14.430673	238	3.5	T (hotspot)	continuous
AQM Praha 4 - Libuš	**ALIBA**	RM Libuš	50.007304	14.445933	301	3.5	SUB	continuous
MS Praha 2 - Karlov	**P1PKAR01**	MS Karlov roof**	50.069167	14.427778	235	28.5	UB	continuous
MS Praha 4 - Libuš	**P1PLIB01**	MS Libuš	50.007778	14.446944	302	10	SUB	continuous
Praha 5 - Stodůlky	**ASTOA**	- - -	50.0461311	14.3314133	309	3.5	UB	continuous
Praha 8 - Kobylisy	**AKOBA**	- - -	50.1221886	14.4675781	269	3.5	SUB	continuous
Praha 4 - Chodov	**ACHOA**	- - -	50.0301706	14.5174503	300	3.5	UB	continuous
Praha 4 - Libuš	**ALIBA**	- - -	50.007423	14.4461857	302	3.5	SUB	continuous

*T = urban traffic, UB = urban background, SUB = suburban background, U = urban

** MS Karlov is placed on the top of the building roof at 28.5 m AGL.

*** The height of wind measurement at the top of the meteorological mast.

F. Calculation of the anthropogenic heat from cars.

As the detailed information on the anthropogenic heat from cars was not available, the goal of this scenario was not to provide an accurate representation of the actual heat flux from cars, but rather to provide an upper bound estimation and then study the sensitivity of the model to the added heat flux.

The total heat flux from cars was estimated as the worst-case scenario from the expected number of cars on the Sokolská and Legerova streets, their estimated running and idling fuel consumption and the energy density of the respective fuels. In order to avoid singularities between the running and idling consumptions, the idling consumption per unit of time $r_0 = 1\,\mathrm{lh}^{-1}$ was subtracted from the reference total consumption $c_{v_r} = 10\,\dfrac{\mathrm{l}}{100\,\mathrm{km}}$ for low speed driving reference speed $v_r = 35\,\mathrm{kmh}^{-1}$ and not fully warmed up engine using a simple formula $\hat{c} = c_{v_r} - \dfrac{r_0}{v_r}$ where $\hat{c}$ is the speed-independent component of consumption per unit of distance. The consumption at speed v (applicable for city driving speeds) per unit of time is then calculated as $r_v = r_0 + \hat{c}v$ which matches the idling consumption r_0 as well as the reference consumption $c_{v_r} = \dfrac{r_{v_r}}{v_r}$. The average street area corresponding to each car was calculated as $a_c = \dfrac{w_s}{n_l}(l_c + l_0 + l_v)$ where $w_s = 21\,\mathrm{m}$ is the total width of the street, $n_l = 4$ is the number of driving lanes, $l_c = 4.5\,\mathrm{m}$ is the reference car length, $l_0 = 1.5\,\mathrm{m}$ is the distance between the cars when stationary and l_v is the speed-dependent stopping distance between the cars which is calculated as $l_v = vt_s$ where $t_s = 1\,\mathrm{s}$. The final anthropogenic heat flux per unit of area was then calculated as $\phi_q = \dfrac{r_v U}{a_c}$ where U is the energy density of the respective fuel. We assumed 40 % of diesel cars with $U = 38.6\,\mathrm{MJl}^{-1}$ and 60 % of petrol cars with $U = 34.8\,\mathrm{MJl}^{-1}$.

In the end, the high estimate heat flux value of $300\,\mathrm{Wm}^{-2}$ was matched to the transportation emission flux of PM$_{10}$ on the Sokolská and Legerova streets at peak traffic hour at $12 \cdot 10^{-9}\,\mu\mathrm{g\,m}^{-2}\,\mathrm{s}^{-1}$. This ratio of $25 \cdot 10^{9}\,\mathrm{J\,kg}^{-1}$ was then used to estimate the heat flux from cars at other locations and at other times.
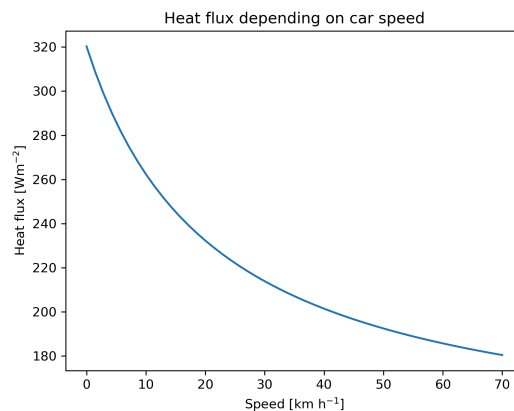
Fig. S14: Dependence of the calculated heat flux produced by cars per unit of area on speed of traffic flow.

G. Comparison of the PALM modeled concentrations of PM_{10} with values observed by sensor stations S14 and S15.
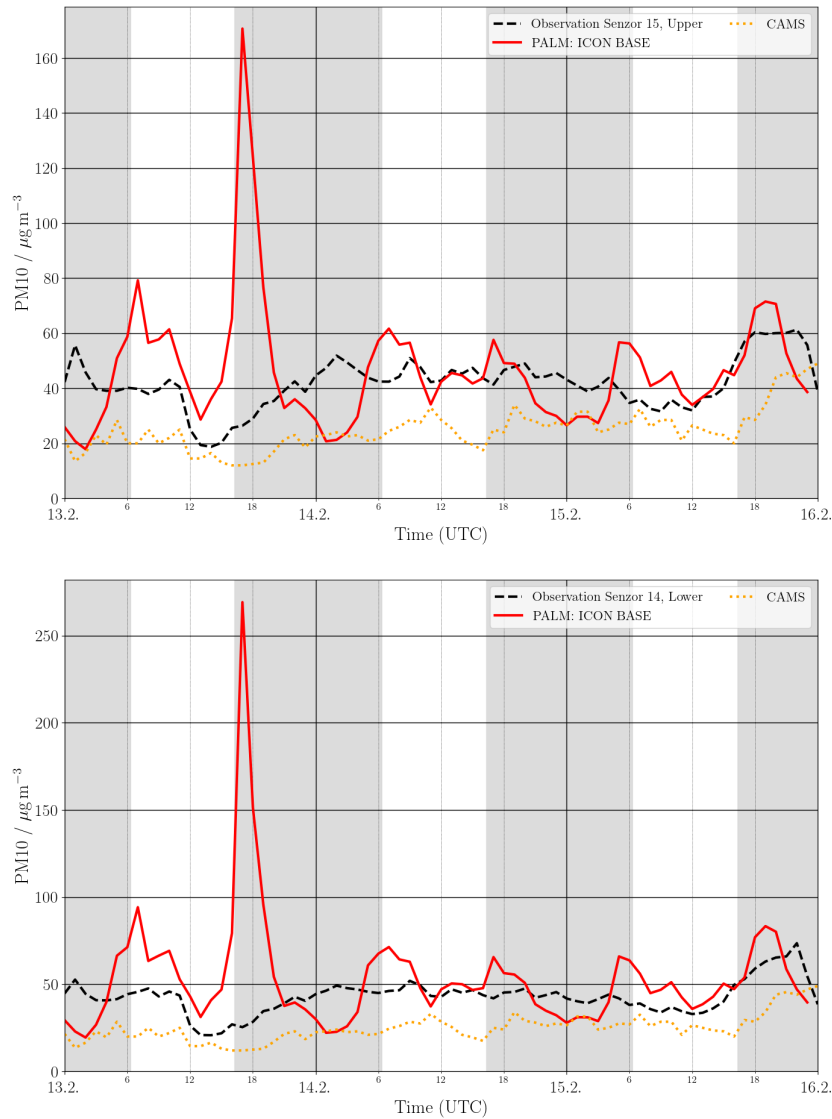

Fig. S15: Comparison of the PALM modeled and observed concentrations of PM10 on the sensors S14 and S15. Observations are represented by the black dashed line and the ICON base scenario is shown by the solid red line. The orange dotted line (CAMS) represents the analysis of the observations and CAMS model used as the BC.

H. Comparison of the PALM modeled concentrations of PM$_{2.5}$ with values observed by ALEGA AIM station.
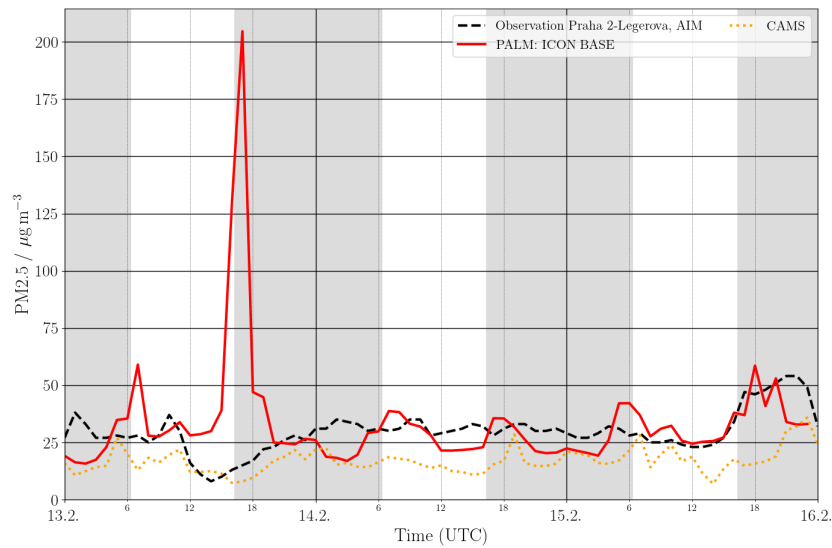
Fig. S16: Comparison of the PALM modeled and observed concentrations of PM2.5 on the AIM station ALEGA. Observations are represented by the black dashed line and the ICON base scenario is shown by the solid red line. The orange dotted line (CAMS) represents the analysis of the observations and CAMS model used as the BC.

I. Modeled and observed profiles of wind speed and wind direction.

Lidar vs PALM
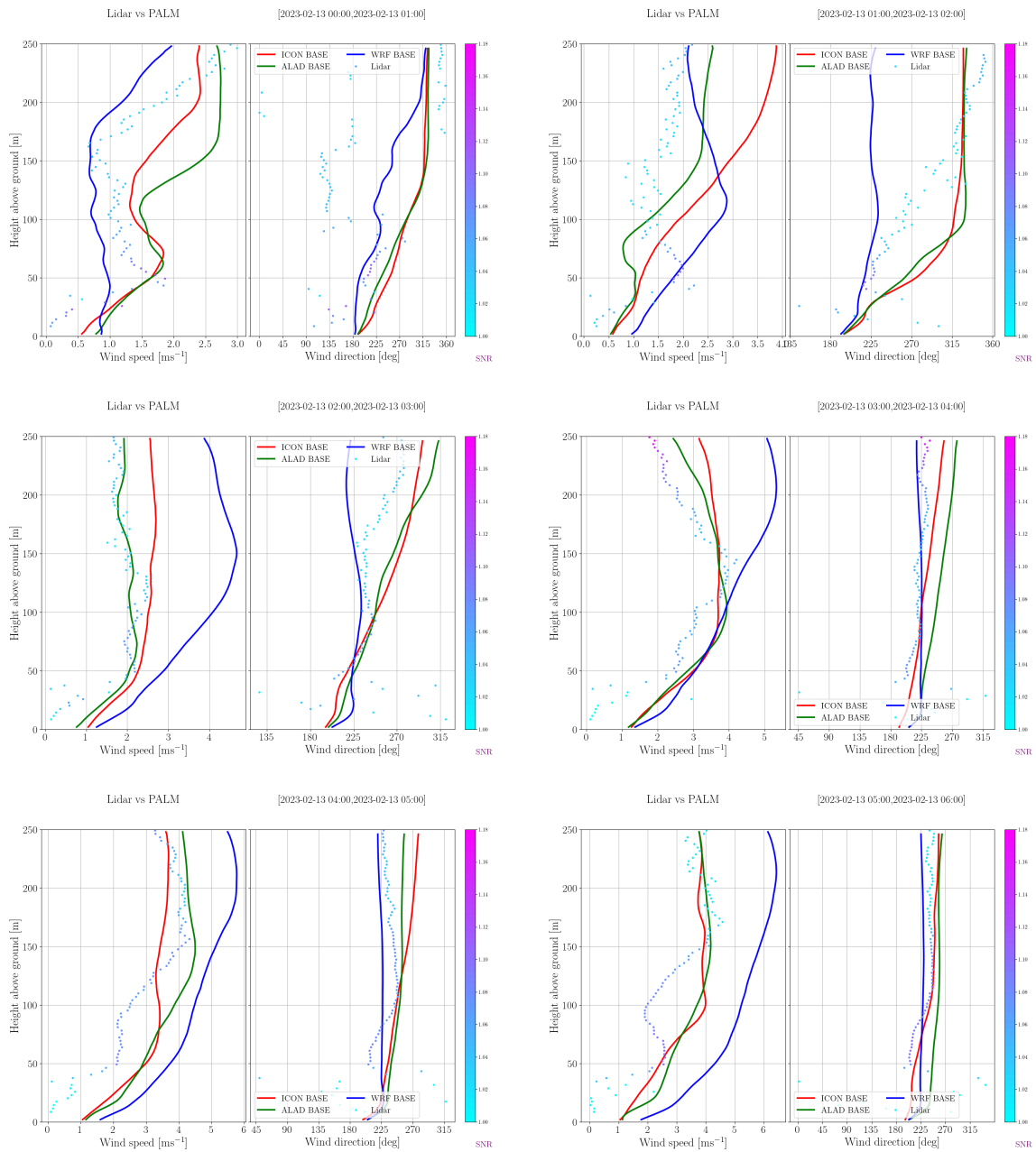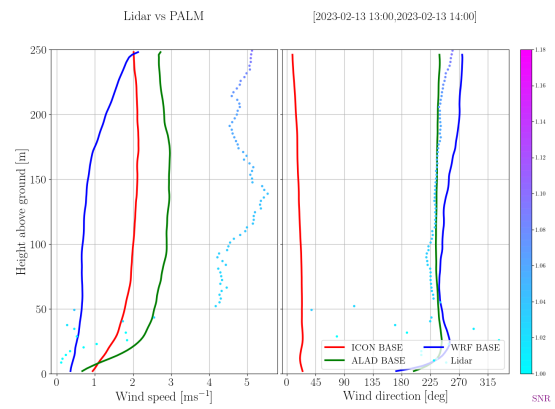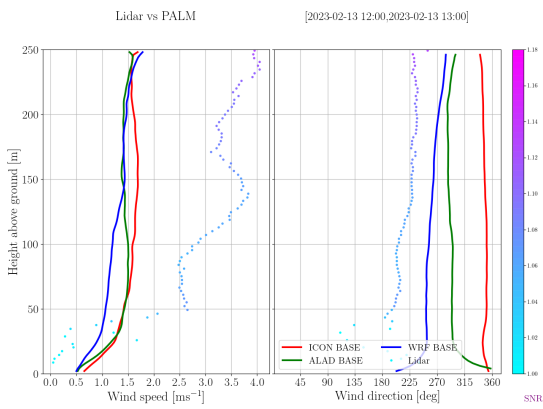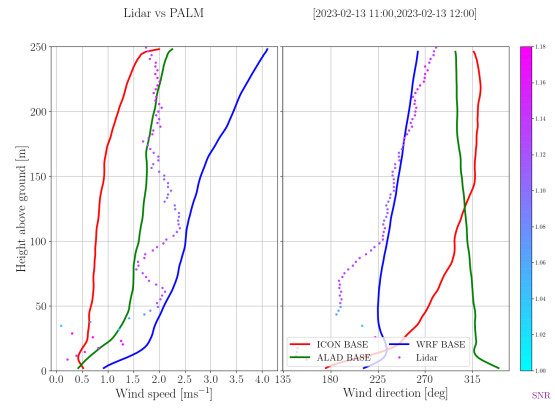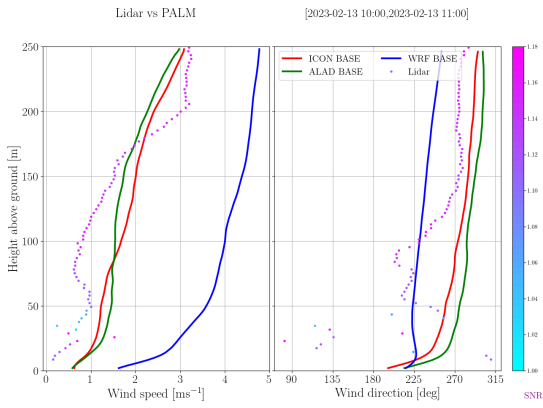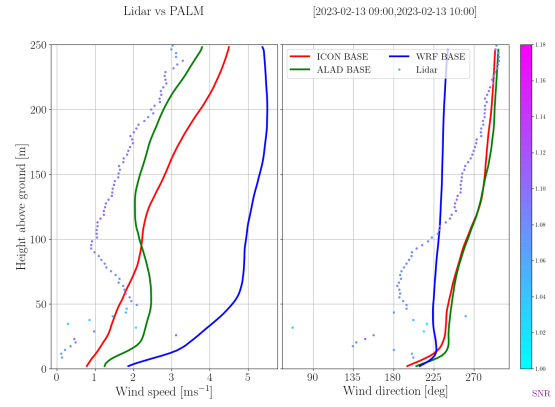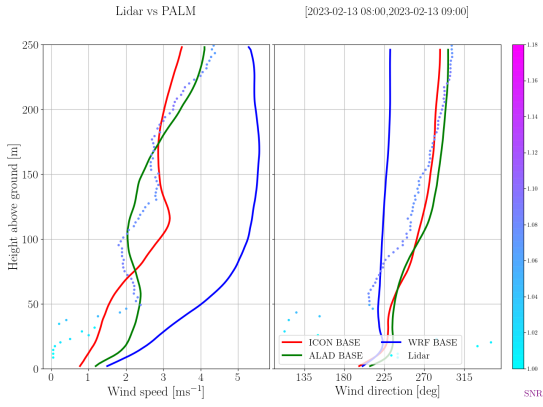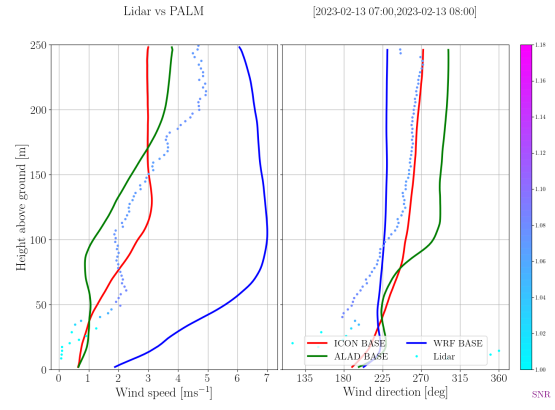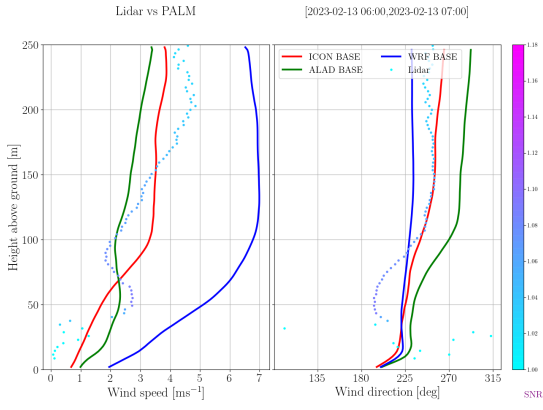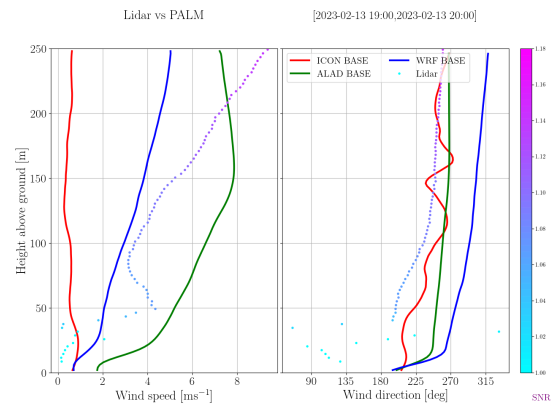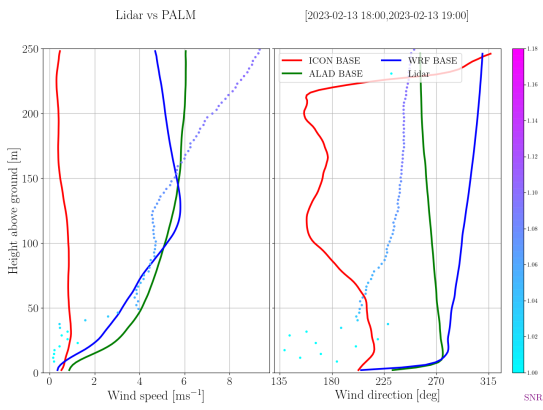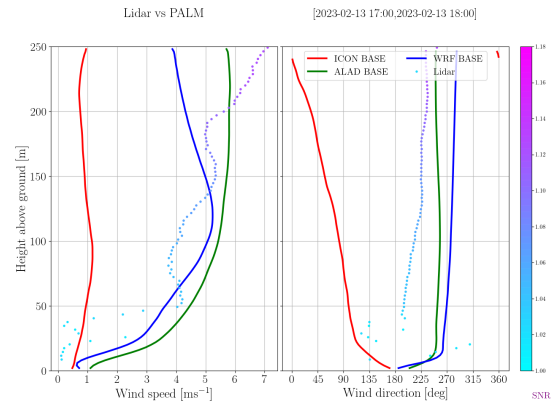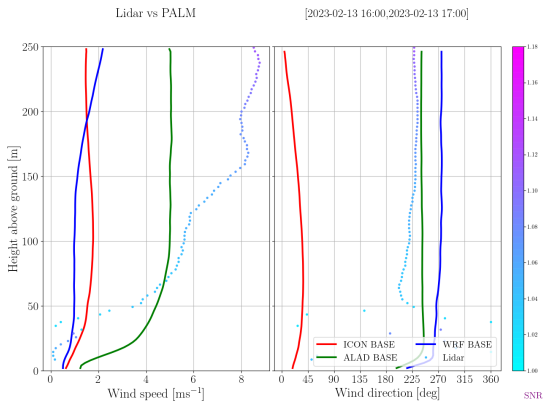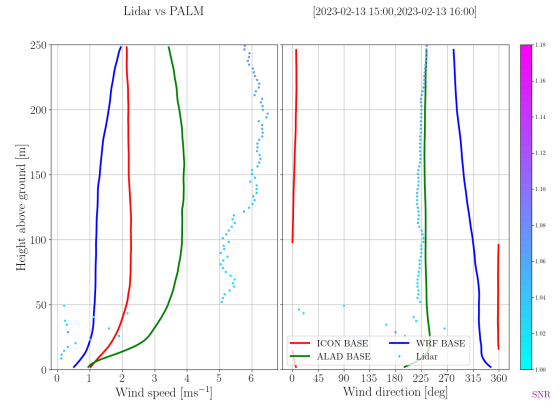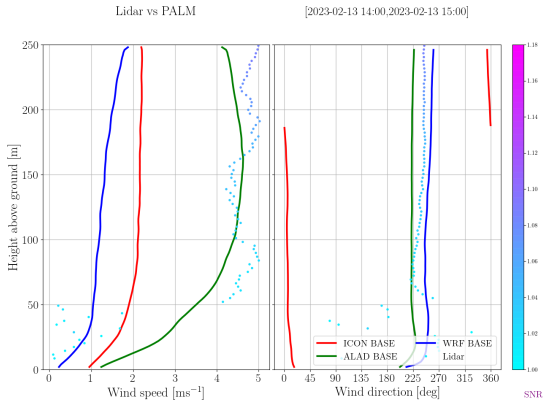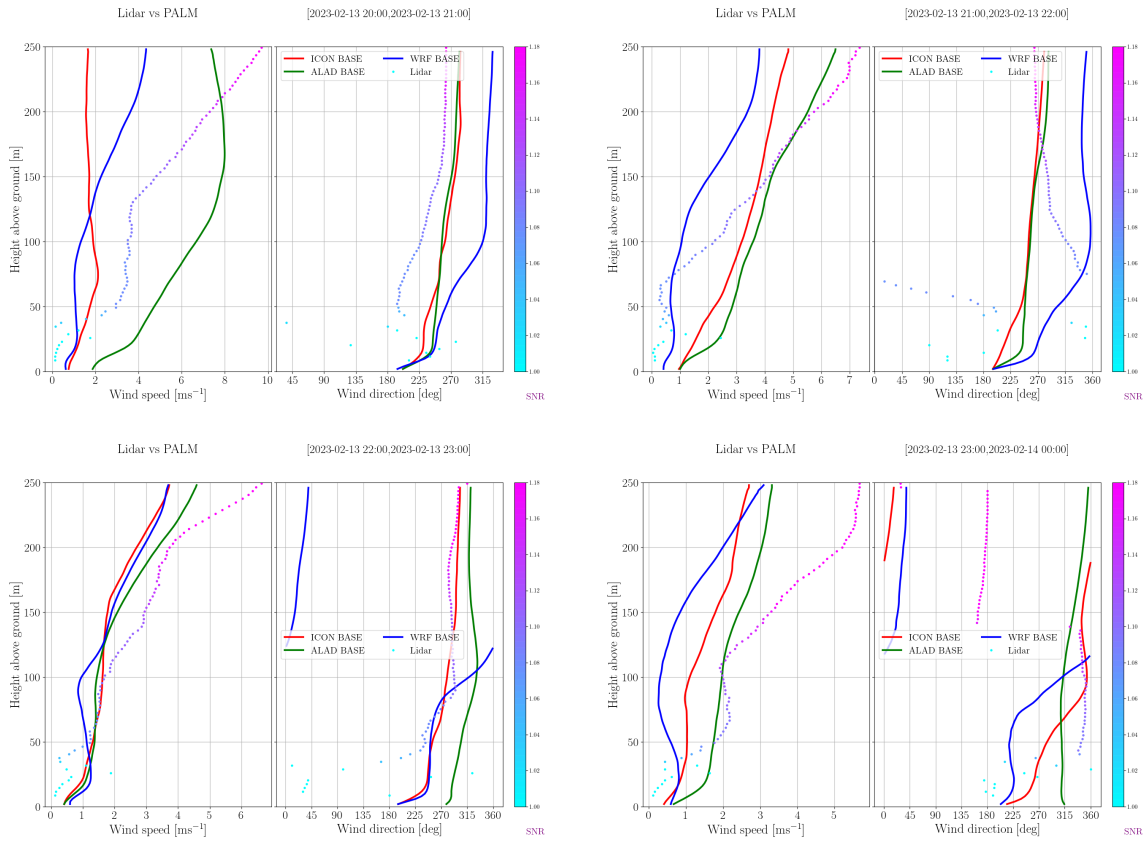
Fig. S17: Vertical profiles of PALM modeled wind speed and wind direction with LIDAR observations for scenarios PALM-ICON, PALM-ALAD, and PALM-WRF for day 13.2.2023. Values represent hourly averages for the hour ending in the given time.
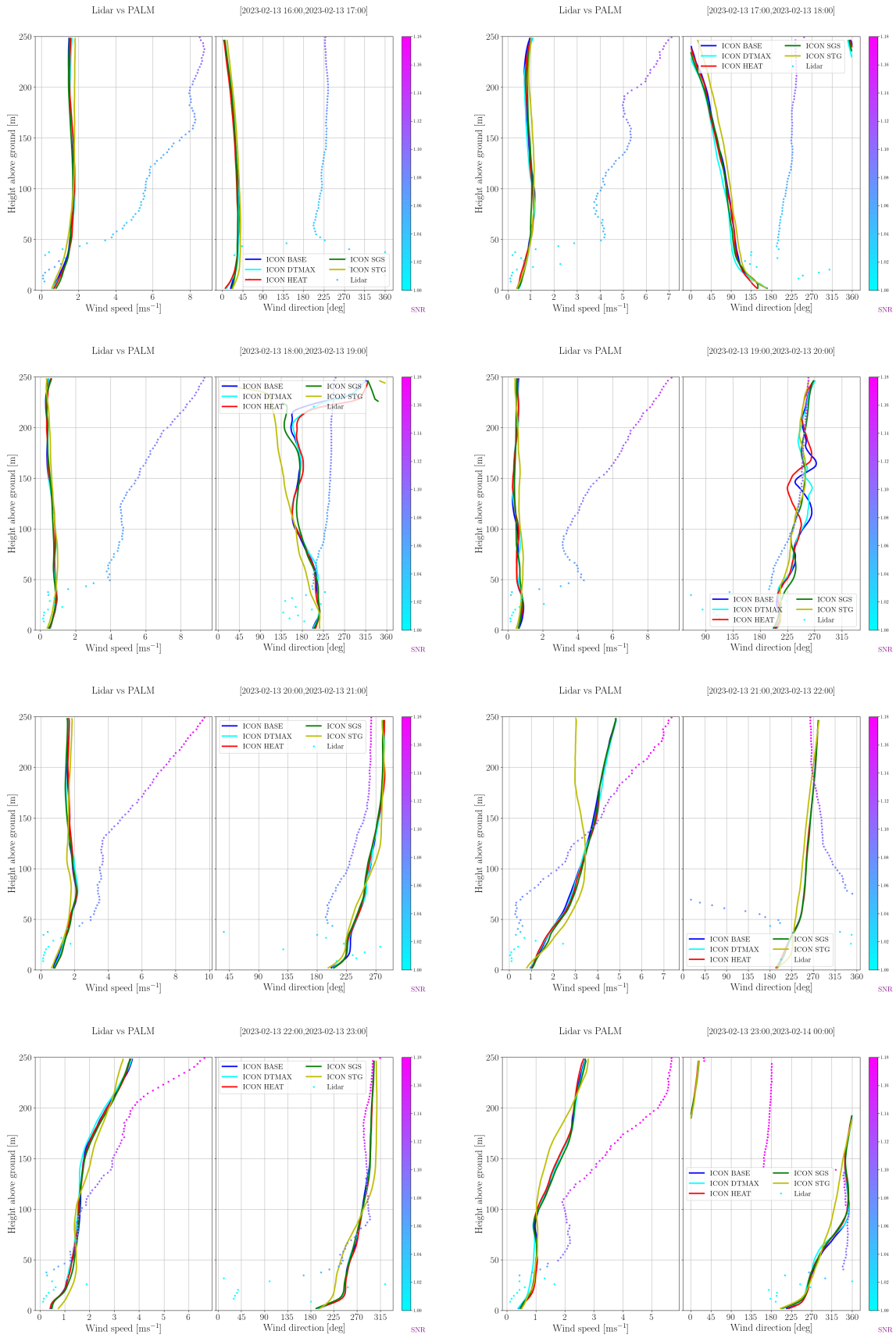
Fig.S18: Comparison of the hourly averaged PALM modeled wind speed and wind direction with LIDAR observations (dotted line) for PALM-ICON (blue) model and HEAT (red), SGS (green), STG (yellow), and DTMAX (cyan) scenarios for day 13.2.2023, hours 16-24 UTC.
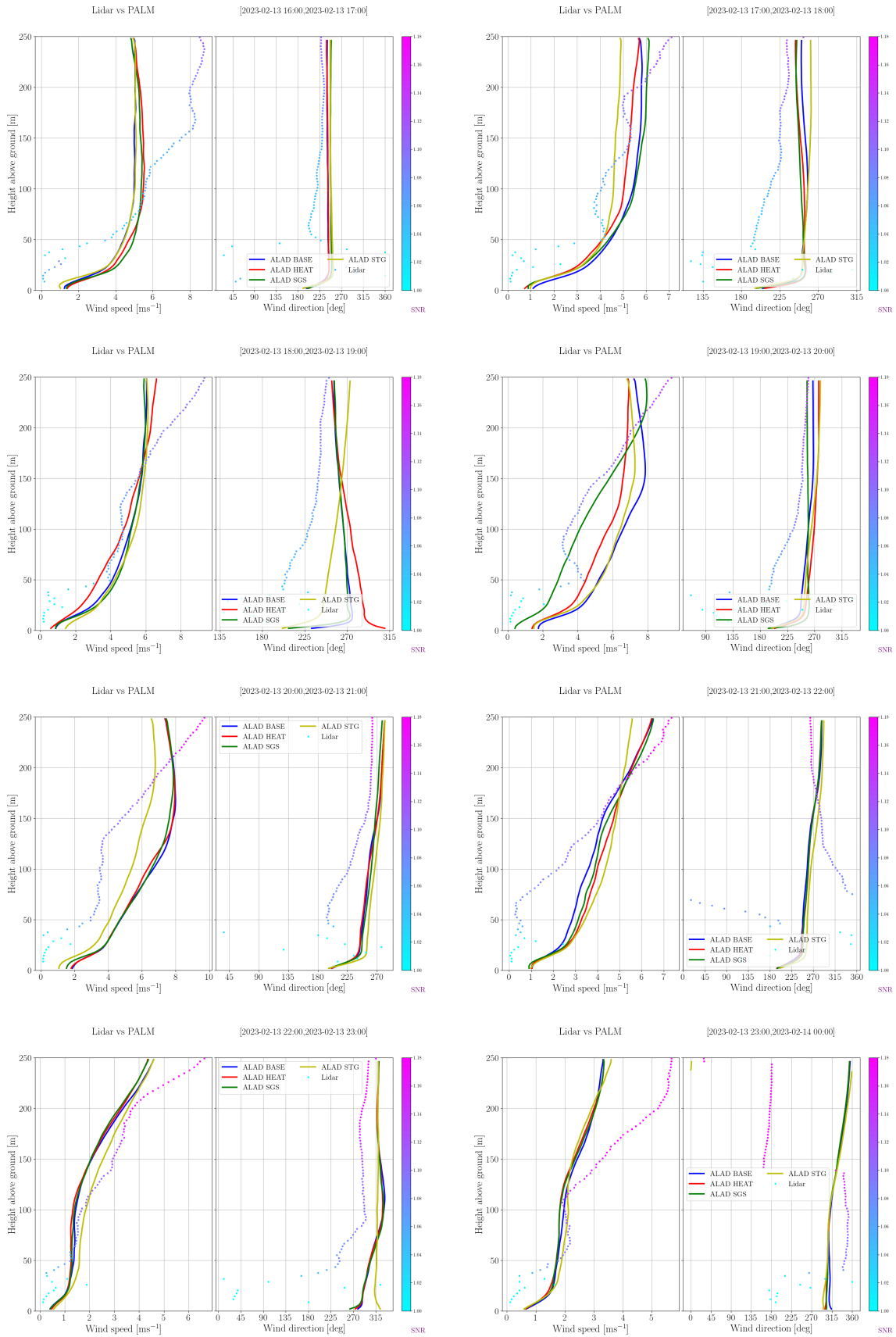
Fig.S19: Comparison of the hourly averaged PALM modeled wind speed and wind direction with LIDAR observations (dotted line) for PALM-ALAD (blue) model, HEAT (red), SGS (green), and STG (yellow) scenarios for day 13.2.2023, hours 16-24 UTC.
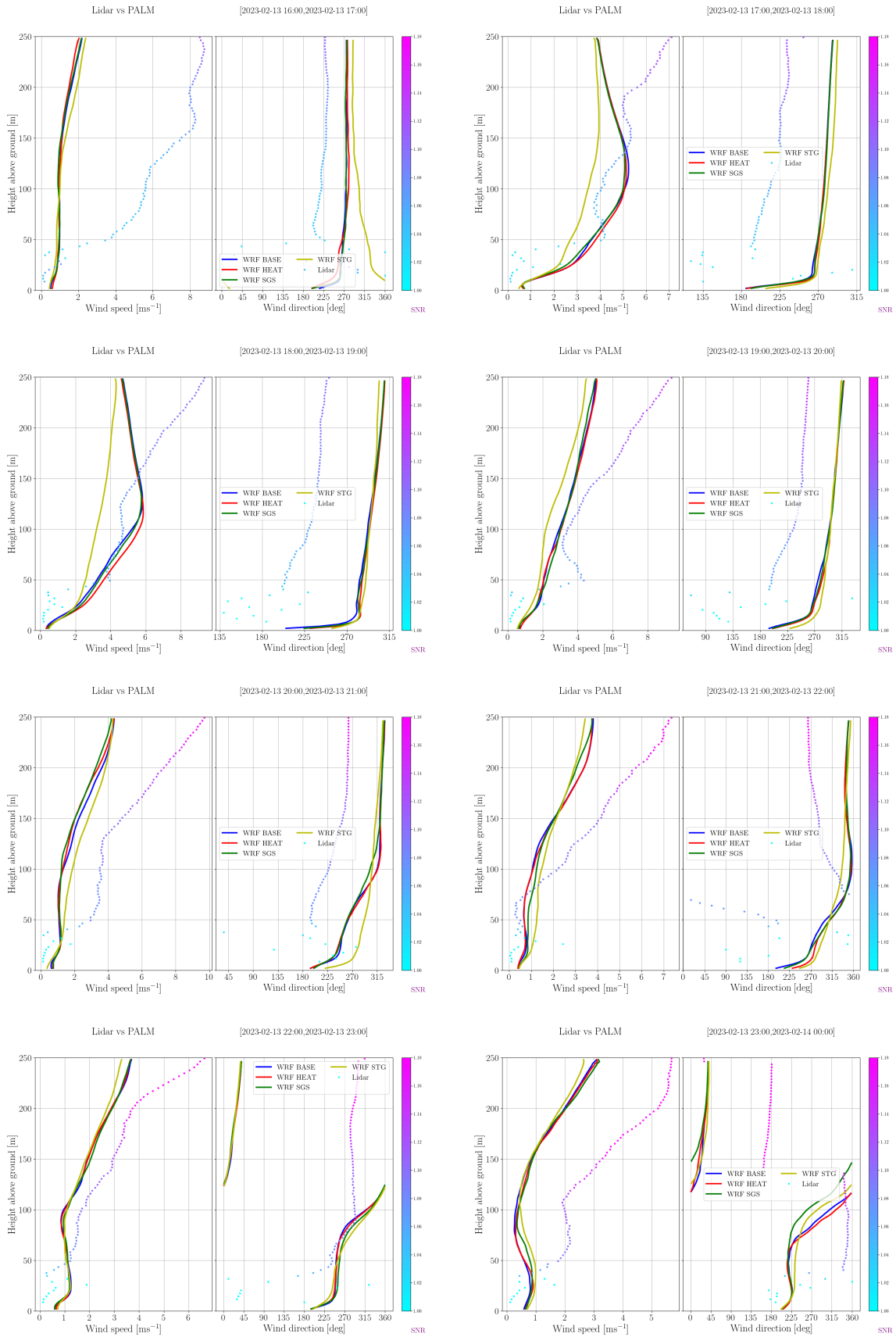
Fig.S20: Comparison of the hourly averaged PALM modeled wind speed and wind direction with LIDAR observations (dotted line) for PALM-WRF (blue) model, HEAT (red), SGS (green), and STG (yellow) scenarios for day 13.2.2023, hours 16-24 UTC.
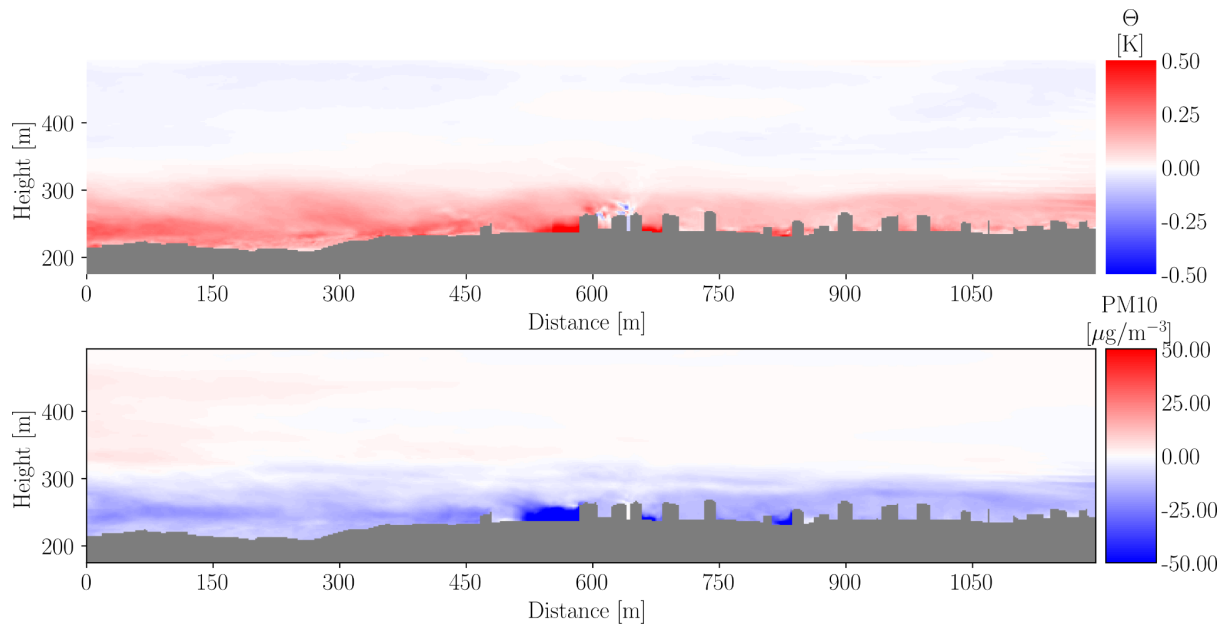
J. Domain cross-sections

Fig. 21: Difference of HEAT minus BASE scenarios for PALM-ICON model on 13 February 2023 at hour 18. The values of air temperature (upper) and concentration of PM10 (lower) on the cross-section through the child domain in the position of ALEGA station are shown.